

T-2267

MAPPING AND FILTERING OF ELECTRICAL POTENTIAL DATA

by

Robert M. Bode

ARTHUR LAKES LIBRARY
COLORADO SCHOOL OF MINES
GOLDEN, COLORADO

CLOSED RESERVE

ProQuest Number: 11016610

All rights reserved

INFORMATION TO ALL USERS

The quality of this reproduction is dependent upon the quality of the copy submitted.

In the unlikely event that the author did not send a complete manuscript and there are missing pages, these will be noted. Also, if material had to be removed, a note will indicate the deletion.



ProQuest 11016610

Published by ProQuest LLC (2019). Copyright of the Dissertation is held by the Author.

All rights reserved.

This work is protected against unauthorized copying under Title 17, United States Code
Microform Edition © ProQuest LLC.

ProQuest LLC.
789 East Eisenhower Parkway
P.O. Box 1346
Ann Arbor, MI 48106 – 1346

T-2267

A thesis submitted to the Faculty and the Board of Trustees of the Colorado School of Mines in partial fulfillment of the requirements for the degree of Master of Science, Geophysics.

Golden, Colorado

Date April 18, 1980

Signed: Robert M. Bode

Robert M. Bode

Approved: Catherine Skokan

Catherine Skokan

Golden, Colorado

Date April 18, 1980

Philip R. Romig

Philip R. Romig

ABSTRACT

The direct-current electrical prospecting method might be improved by measuring the electrical potential of a bipole source and then applying filtering and interpretation procedures already developed for gravitational and magnetic prospecting. A field program was carried out in the northern San Luis Valley of Colorado. Potential differences of a bipole source were measured and then added up from a reference level to get the potential. Maps of the potential and apparent resistivity were then generated. The resistivity map generally agreed with the work of previous investigations (Jordan, 1974; Arestad, 1977; Keller, in Romero and Fawcett, 1978; Mamah, 1979).

The potential map was fit to low order surfaces, and filtered with a downward continuation filter. The surface fitting worked very well, and seemed to be equivalent to a downward continuation. Sixth, eighth and tenth order surfaces were used, and each showed a high in the western part of the map and a north-south trending low in the center. The high in the west corresponds to volcanics that are overlain by a thin cover of alluvium, and the low corresponds to the deepest part of the valley.

Downward continuation did enhance the two anomalies, but had a tendency to filter out the low on the tenth order surface. Better filtering methods could improve the down-

ward continuation. The manipulation and interpretation of the surface fitting and downward continuation would be aided if Fourier analysis was used to see how the wavelength content of the maps is being altered.

This method of prospecting worked fairly well for the large scale structures, but was unable to show the finer structures in the basement. To see the finer structures, better field coverage and improved filtering methods must be used.

The mapping of the electric potential gave information about the subsurface in two ways, that of resistivity maps, and secondly the potential maps themselves. This method has improved the direct-current mapping methods by giving the added information about the subsurface which was obtained from the potential maps. Also, with improved data processing and modeling it should give even more information.

TABLE OF CONTENTS

ABSTRACT	iii
LIST OF ILLUSTRATIONS AND FIGURES	vi
ACKNOWLEDGEMENTS	viii
INTRODUCTION.	1
THE POTENTIAL	4
FIELD SURVEY.	11
DATA REDUCTION	17
RESISTIVITY	25
SPATIAL FILTERING	30
INTERPRETATION	51
CONCLUSIONS	65
APPENDIX I	67
REFERENCES	75

LIST OF ILLUSTRATIONS AND FIGURES

Figure

1. Array	6
2. Theoretical model	8
3. Thesis' area	12
4. Example of a record with tellurics	16
5. Example of a record with no noise	18
6. Map of the potential	21
7. Scatter plot of potential	22
8. Map of potential with additive constant	23
9. Map of the potential after subtraction of a half- space of the average resistivity	24
10. Map of the geometric factor	26
11. Map showing areas where the resistivity was edited	28
12. Map of apparent resistivity	29
13. Sixth order surface	34
14. Sixth order residual	35
15. Eighth order surface	36
16. Eighth order residual	37
17. Tenth order surface	39
18. Tenth order residual	40
19. Filter grid for downward continuation	42
20. Sixth order surface continued down one mile.	43

Figure

21.	Sixth order surface continued down two miles.	44
22.	Eighth order surface continued down one mile.	46
23.	Eighth order surface continued down two miles	47
24.	Tenth order surface continued down one mile	48
25.	Tenth order surface continued down two miles	49
26.	Map of apparent resistivity	52
27.	Map of apparent resistivity from Jordan	53
28.	Map of apparent resistivity from Jordan	54
29.	Map of apparent resistivity for N-S bipole	55
30.	Map of apparent resistivity for E-W bipole	57
31.	Apparent resistivity map from Keller	58
32.	Sixth order surface continued down one mile	59
33.	Crossections	60
34.	Gravity model	61
35.	Geologic crossections	62
39.	Crossection of the sixth order surface continued down one mile	64
Table 1.	Filter coefficients for downward continuation	41
Plate 1.	Map of station locations.	

ACKNOWLEDGEMENTS

I would like to thank Dr. C. Skokan for her help and guidance as thesis advisor. I am grateful to Dr. G. V. Keller and Dr. C. H. Stoyer for their help and suggestions as committee members. I appreciated the suggestions, criticisms, and help of Dr. David Buttler. Thanks goes to Fred Berkman for the surface fitting program used.

I am grateful to Luke Mamah, Yo Katahira, Nancy House, and the 1978 Saguache field camp students of the Geophysics department of the Colorado School of Mines. A special thanks goes to all my friends and fellow graduate students for their comments and moral support.

I am grateful to the Department of Health, Education, and Welfare for financial support through Mining and Mineral and Mineral Fuel Conservation Fellowships. I also appreciated the financial help of the Geophysics Fund Inc., which made the field program possible.

INTRODUCTION

Electrical prospecting methods have been used increasingly in the past few years. They are being applied to ground water, geothermal, mining, and oil exploration problems. With this rise in the use of electrical methods there has also been an increase in research to improve the electrical methods. The object of the research described in this report is to develop and improve field, modeling, and interpretation techniques.

Direct-current electrical methods are probably the best understood of the electrical prospecting methods, but they suffer from several problems of which field procedure is one. For direct-current electrical prospecting methods it is usually necessary to use cables that may be many kilometers in length if you wish to see a target only a kilometer or two in depth. Also, there are problems with current leakage and safety with these long cables. Laying these long cables in the field is a slow and expensive task. The developing of quicker less expensive methods of prospecting has resulted in the development of the dipole methods of electrical prospecting (Alpin and others, 1966; Keller, 1966; Keller and others, 1975).

The dipole techniques originally used short grounded wires for source and receiver, in which the length of the

dipoles was far shorter than the source and receiver separation (Alpin, 1966; Keller and Frischknecht, 1966). Later the dipole techniques were modified by using a fixed bipole source and a roving dipole receiver (Keller, 1966). The bipole source was much longer than the length of the dipole receiver. As the bipole-dipole method developed it became more sophisticated, and crossed receiver dipoles were used to calculate the total electric field (Keller and others, 1975; Zohdy, 1978). The method soon made use of two orthogonal sources, and the field procedure became more complex. With all these developments in the field method and theory, there was little done on the modeling and interpretation. The modeling consisted of finite difference modeling, with most of the interpretation depending on resistivity and conductance maps. So the objective of surveys was to map the areal extent of conductivity or resistivity anomalies. This lack of modeling and interpretation methods has resulted in limited use of these techniques. Also the increasing complexity of the field work has increased the cost of these types of surveys.

These problems with the method have made it a suitable area for further research. By using information about the electric field it should be possible to find ways to improve the field method, the modeling, and the interpretation of data from this kind of method. One of the interesting things about the electric field is its associated potential

field. This potential field may possibly be interpreted using the same methods as are used for other potential fields such as gravity or magnetism. In both the gravitational and magnetic methods, ways have been developed for locating structure, determining depth to basement, and enhancing the expression of an anomaly.

The methods used in gravity and magnetics are upward and downward continuation, gradients, second and fourth order derivatives, and low-pass and high-pass filtering. The first application of these methods to electrical prospecting was by Amalendu Roy (1966). Since the work of Roy, the only other published work applying the methods of potential data processing to electrical prospecting was the work of House (1979). It was proposed by Keller (1978) to measure the potential of a bipole source, and to then apply a downward continuation filter to the data. A field survey was carried out in the San Luis Valley of Colorado. The data were to be then gridded and fit to a low order surface. Downward continuation of the surface would hopefully give information about the structure of the electrical basement of the valley.

THE POTENTIAL

The electrical potential field of our source and a method of modeling the earth must now be expressed. The electrical potential field is a conservative field, and behaves in a similar manner as do the potential fields of gravity and magnetism (Kellogg, 1929). Because it is similar to the gravitational and magnetic fields, it should be possible to interpret electrical potentials in the same manner as gravitational and magnetic data. The sources of the electrical potential are equivalent charges that locate on surfaces or boundaries of bodies of different resistivity. If these charges can be located in space, you also would locate the boundaries. By locating these boundaries you would identify the structure of the earth. A method of inverting the anomalous field, to find the sources of the field, will give a model of the earth. In gravitational and magnetic prospecting this is done by downward continuation of the field.

The potential for a direct-current bipole source can be derived from the superposition of the potentials from two point sources. The potential for a point source on a half-space is:

$$U = \frac{\rho I}{2\pi R}$$

U= the potential,

ρ = the resistivity of the half-space,

I = the source current,

R = the distance from the measuring point
to the source.

The potentials, at point e, due to the two electrodes of the source are (Figure 1):

$$U_A = \frac{\rho I}{2\pi R_1} \quad (2)$$

and,

$$U_B = \frac{\rho I}{2\pi R_2} \quad (3)$$

where U_A and U_B are the potentials due to the respective electrodes. These two potentials are superposed to get the potential of the bipole source, which is:

$$U_S = \frac{\rho I}{2\pi} (1/R_1 - 1/R_2) . \quad (4)$$

For ease of calculation this can be normalized to the distance R_1 :

$$U_S = \frac{\rho I}{2\pi R_1} (1 - R_1/R_2) . \quad (5)$$

This is the expression for the potential of a bipole on a half-space.

We must now see if there is some justification for the way we intend to treat the electrical potentials. Modeling of the field due to an arbitrary shaped body has been dealt with by Alfano (1959), Keller and Frischknecht (1966), and Barnett (1972). I will follow closely the development of

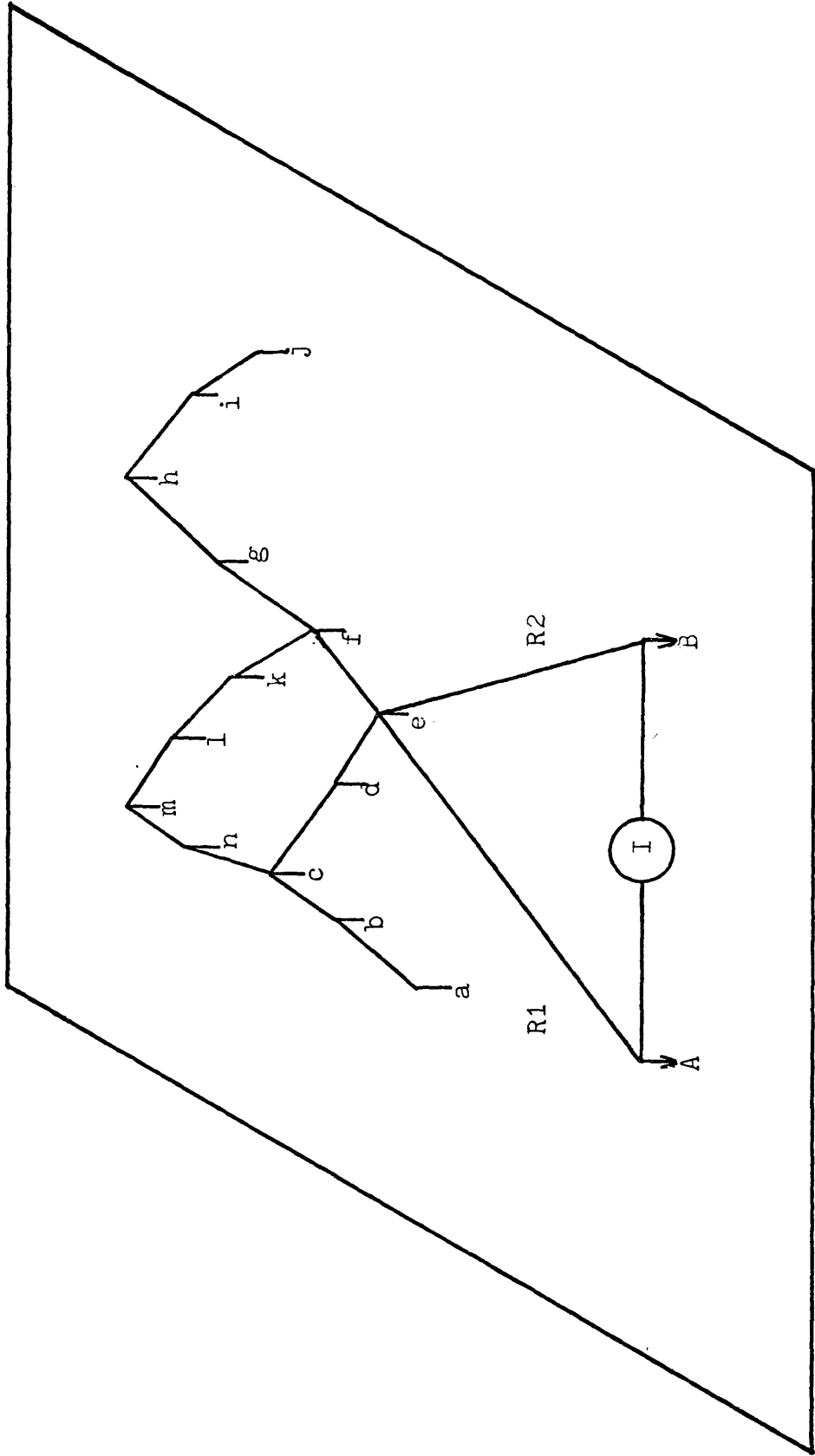


Figure 1. Array of source bipole and dipole receivers.

Keller and Frischknecht (1966).

The model we are looking at is that of a semi-infinite medium of resistivity ρ_1 , with an arbitrarily shaped body of ρ_2 inside it (Figure 2). We will solve for the potential using a single source electrode at A and a measuring point at M.

For direct-current flow the following equations must hold:

$$\nabla \cdot \vec{j} = 0 \quad (6)$$

\vec{j} = the current density,

∇ = the operator Del;

$$\vec{E} = \rho \vec{j} \quad (7)$$

\vec{E} = the electric field vector,

ρ = the resistivity.

Combining equations 6 and 7,

$$\nabla \cdot \frac{\vec{E}}{\rho} = \frac{1}{\rho} \nabla \cdot \vec{E} + \vec{E} \cdot \nabla (1/\rho) = 0 \quad (8)$$

This allows us to write the expression defining potential:

$$\vec{E} = -\text{grad } U \quad (9)$$

U = potential.

Combining the last two equations,

$$\nabla \cdot \frac{\vec{E}}{\rho} = \frac{1}{\rho} \nabla \cdot \nabla U + \nabla U \cdot \nabla (1/\rho) \quad (10)$$

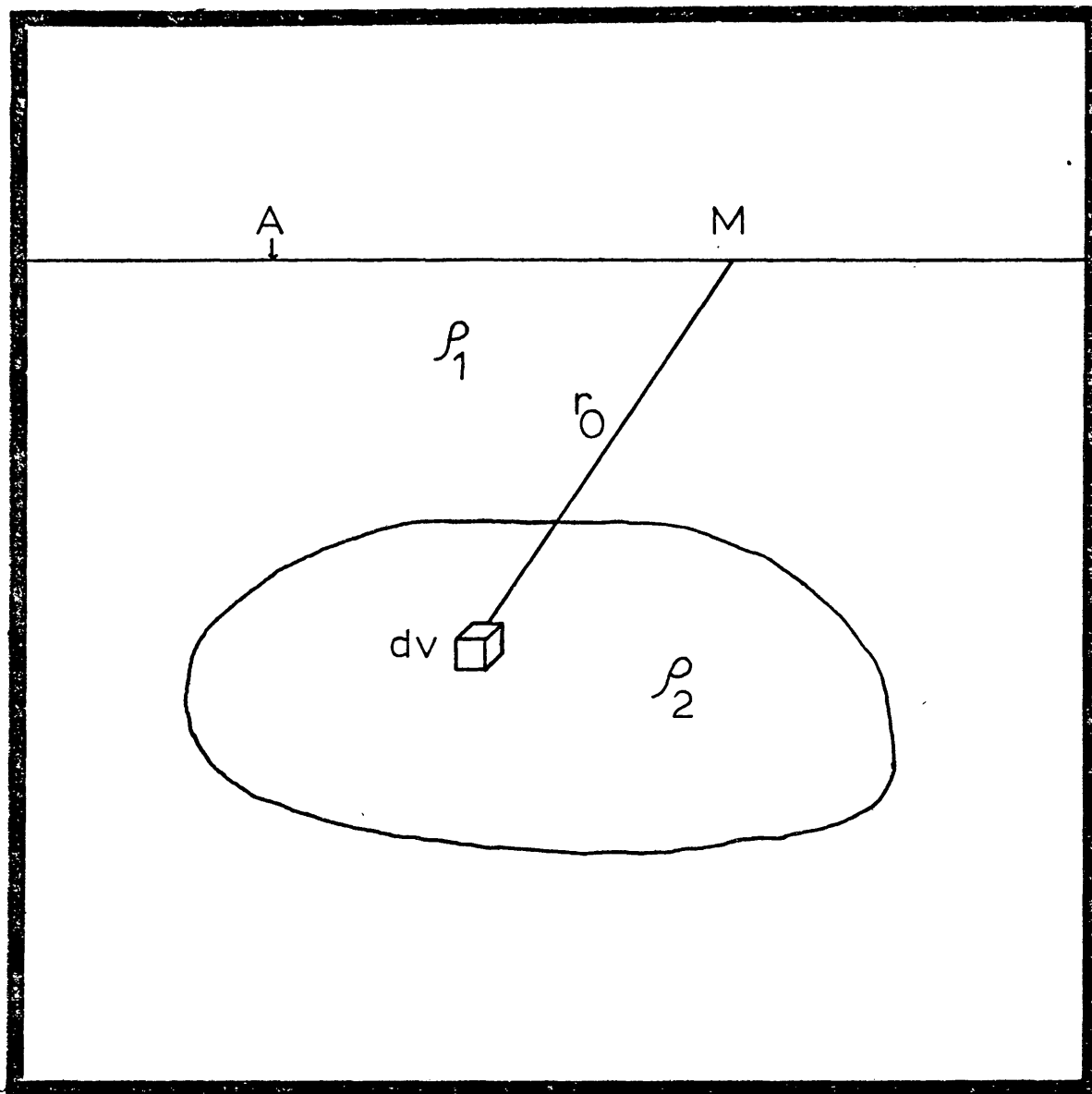


Figure 2. Arbitrarily shaped body of resistivity ρ_2 in a half-space of resistivity ρ_1 , with a point source and a receiver.

This may be rewritten as:

$$\nabla^2 U = -\rho(\nabla U \cdot \nabla (1/\rho)), \quad (11)$$

which is a form of Poisson's equation. This equation represents the effect of sources in the medium.

The solution for Poisson's equation is:

$$U = \frac{1}{4\pi} \iiint \frac{-\rho \nabla U \cdot \nabla (1/\rho)}{r_0} dv, \quad (12)$$

where r_0 is the distance from the measuring point to the elemental volume. But this expression is zero unless ρ is non-homogeneous, since for a homogeneous earth $\nabla (1/\rho) = 0$, and the earth model is only non-homogeneous on boundaries or where there is a gradient in resistivity. So the source of the field acts like a surface distribution of charge in a homogeneous medium. This reduces the integral to a surface integral of a surface density of equivalent charges:

$$U = \frac{1}{4\pi} \iint \frac{\sigma}{r_0} ds, \quad (13)$$

where σ is equivalent charge per unit area.

Mathematically, our disturbing field can be thought of as being due to equivalent charges located where the surface of the disturbing body was, but now in a homogeneous half-space of ρ_1 . The enclosed volumes do not contribute to the disturbing field. These equivalent surface charges can either counteract or add to the source field

depending on whether or not the reflection coefficient is positive or negative. It is these equivalent surface charges that will give the model of the earth. If you can invert the anomalous field to locate these equivalent charges, you will get a model of the earth.

FIELD SURVEY

During the summer of 1978 a field program was carried out in the Northern San Luis Valley of Colorado (Figure 3). The program was part of the Colorado School of Mines field camp. In addition to the field camp, data was also taken during the last two weeks of August of the same year.

The San Luis Valley is part of the Rio Grande Rift, and is a graben situated between the Sangre de Cristo mountains on the east and the Sawatch mountains and Bonanza volcanic complex on the west. Initial graben development began in the late Miocene and Pliocene (Romero and Fawcett, 1978). The valley is bounded on the east by the Sangre de Cristo fault, and the valley is thought to be an eastward-tilted block (Knepper, 1974). The basement beneath the valley floor is made up of Precambrian and Paleozoic rocks, and the valley fill is composed of debris from the surrounding mountains (Romero and Fawcett, 1978). There are several faults that trend northwestward that are referred to as the Villa Grove fault zone (Knepper, 1974). A possible sub-graben Northeast of Mineral Hot Springs has been reported by Jordan (1974) and Stoughton (1977).

The valley is of interest because of the vast quantities of ground water it contains, and the possibility of economically exploiting its geothermal system.

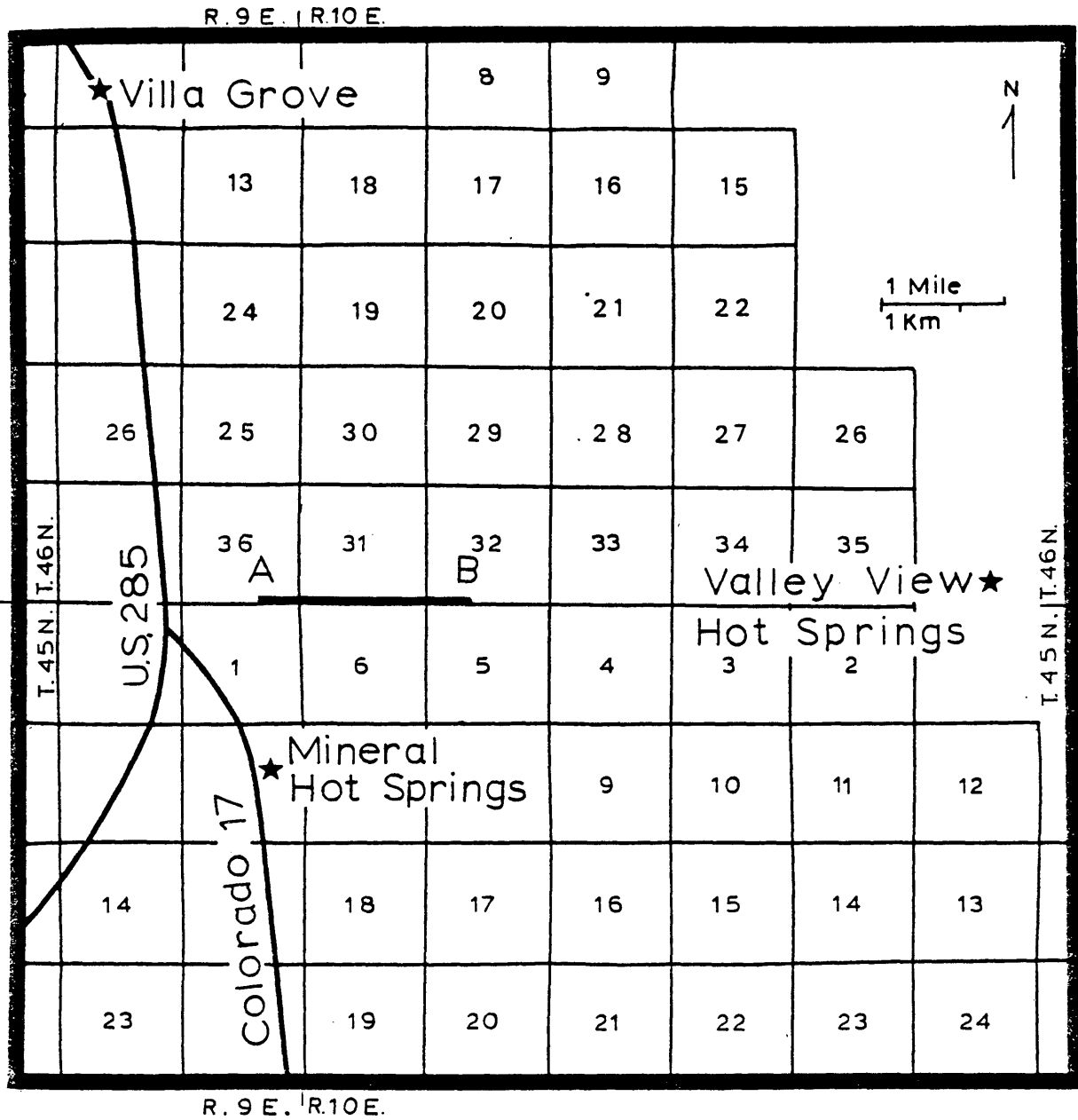


Figure 3. Area of the field program in the northern San Luis Valley of Colorado. AB is the bipole source.

For the field survey, the source was located on an east-west road, and two culverts were used as electrodes (AB in Figure 3). The source was 2.7 kilometers long. A three-phase, 27 kva Onan generator was used as a prime power source. The output of the generator was rectified, to approximate direct-current, and switched positive and negative to generate a square wave. The wave form was asymmetric, with the one side being 7 seconds long and the other 15. This enabled the polarity of the received signal to be determined. Also by switching positive and negative the signal was doubled in amplitude.

The receiver consisted of two bipoles and a recording system. The bipoles were two porous pot electrodes linked to the recording system by 18 gauge wire. The length of the bipoles varied between 1000 and 1300 feet. Because of the method of measurement, the absolute length of the bipole need not be known. This is because the station location or point is all that is needed for determining the resistivity, and that the potential was the object of the measurement, not the electric field. Three porous pots were used so that two sequential bipole measurements could be made simultaneously. The central pot of these three was a common. Potential differences of the bipoles were measured and recorded. The signal received was amplified, filtered to reject sixty hertz noise, and then recorded on a chart recorder.

During the survey it was sometimes necessary to put a voltage divider between the amplifier and the chart recorder to increase the range of the system. Eventually the ratio of input to output voltage would be used to take out the effect of these voltage dividers. Also, the data would be normalized to a gain of one.

The field procedure consisted of laying out the two bipoles, and recording ten to twenty cycles of signal. After a station was recorded, the gains, location, date, and station number would be recorded on the record. The stations were put on a map using landmarks and the odometer of the recording truck for positioning. The bipoles would then be pulled so that the trailing electrode would change places with the leading electrode. In Figure 1, after recording signals from bipoles ab and bc, the wire would be pulled forward to measure bipoles cd and de. This method of leap frogging was conducted on the roads of the area, and resulted in a dendritic pattern of stations. The station locations are in plate 1.

To get a reference point from which the potential differences could be added, it was necessary to have some of the stations go out until the signal would fall to near zero. This approximated infinity and then the potential differences could be added from this point. The potential at this far point was assumed to be zero.

Several types of noise were encountered during the

survey. These noises included tellurics, induction, sferics and noise from power lines. Tellurics were by far the greatest noise problem, and on some records effectively hid the signal (Figure 4). The induction and power line noises were not much of a problem, and were probably negligible. Also, sferics are of such a short duration, that they were of little concern. Occasionally there were also difficulties with the chart recorder response. When in doubt about the quality of the station it was rerecorded or reoccupied. Most of the reoccupied stations resulted in similar data to the first recordings, and the problem can be attributed to array geometry.

There were 158 stations recorded, of which only 132 were used for the interpretation. This provided 264 actual data points for the interpretation. The reason data were omitted was that they fell outside of the actual area finally used in the interpretation.

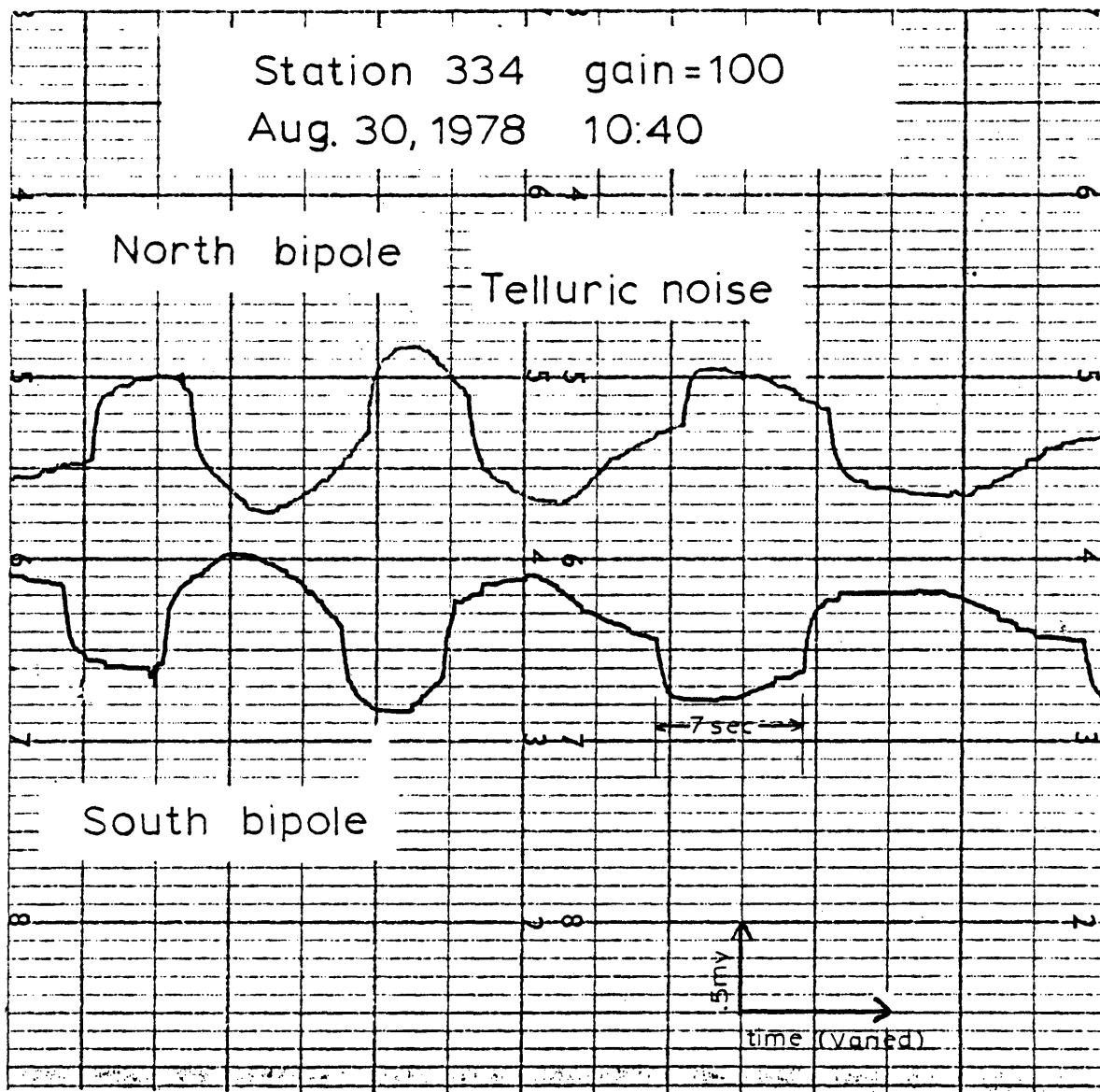


Figure 4. Example of a receiver record showing telluric noise.

DATA REDUCTION

The field records needed to have the offsets turned into voltages, and telluric noise had to be filtered out. To convert the offsets to voltages a simple average of each cycle was used. This was done with the noiseless records (Figure 5). When the record had telluric noise (Figure 4), a graphical method of filtering out the noise was used. This was accomplished by photostating the record and then superposing it on the original record. Then the photostat was shifted half of a cycle in time, and the signals were lined up so that it approximated the best fit. The amount that the photostat had to be shifted up or down was the value of the square wave amplitude. In some areas the tellurics were so bad that a guess had to be made between a maximum and a minimum offset on the record. Sometimes it was only possible to fit parts of the record. In this case the value for the parts was averaged with a simple average.

The polarity was determined by setting a convention, that the signal of the first station was positive. After that, the traces with the same polarity were positive, and those with reversed polarity were negative. But this assumed that the input wire polarity and the source polarity had never been changed. At three different points it is known or assumed that the wires had been tampered with,

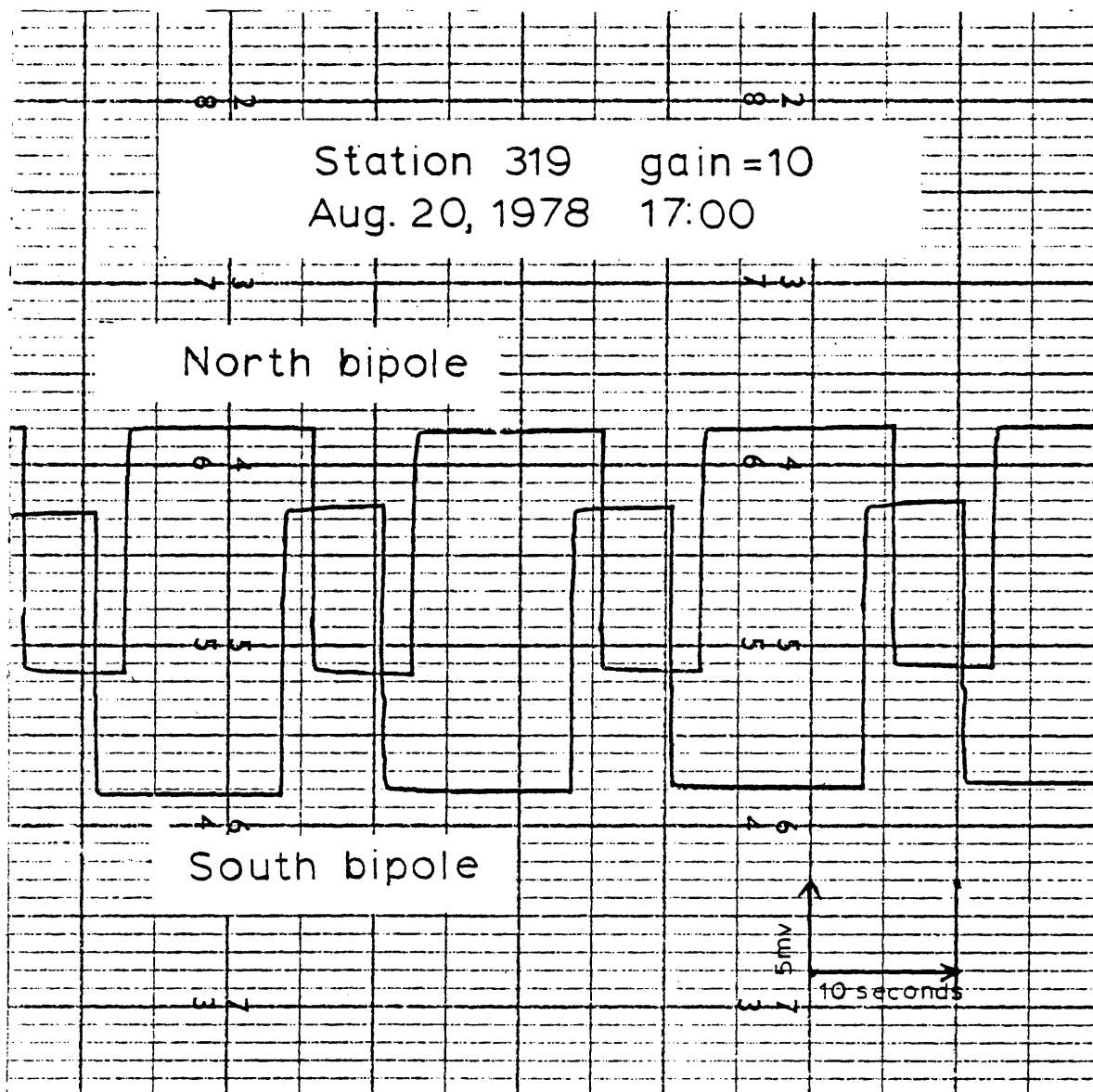


Figure 5. Example of a receiver without noise.

and the polarities were reversed to correct for this.

The current of the source for each station was determined by taking a simple average of the square wave of the current record for that station. The voltages, current, station number, and x-y coordinates of each receiver electrode, were put into a file for processing on the Colorado School of Mines PDP 10 computer.

The voltages now had to be normalized to a standard voltage. This was originally going to be done by using the calibration from the field records, but due to the calibration not being reliable, another way had to be found. The final data set used, was normalized to a gain of unity by dividing by the amplifier gain and multiplying by the value of any voltage divider that may have been present. The calibration for the system at a gain of unity was used so that the values would be in volts. This method appeared to work well.

To calculate the potential referred to a common level, the voltages had to be added up from our farthest station, the farthest station being the station where the signal fell off to nearly zero. This was where the signal could not be picked out of the noise. The station was then assumed to be infinitely far from the source, and from here potential differences can be added up to determine the potential. Prior to the summation, the voltages can be normalized to the current strength to take out the effect of

variations in the source. Both normalized and non-normalized data were tried, and I found little difference in the two. This is probably due to the current being relatively constant. The non-normalized data were used for the interpretation (Figure 6).

The data now needed to be checked to see if they were precise enough to be meaningful. At junction points of closed lines, the potential should be the same, and by checking these points, an estimate of the error may be made. The error at the junction points varied between 6 and 20 percent.

The data were off by an additive constant because of the assumption of adding from infinity. This constant was determined by fitting a least squares line through the data, and then adding constants until the root mean square error was a minimum. The constant finally used was .0118 (Figure 7). The deviation from a straight line by some of the points is expected, otherwise, the data would represent a half-space. This constant did not alter the shape of the potential map, but it did alter the values (Figure 8).

The data were also checked to see if there were any anomalies. The method that worked best was that of subtracting the effect of a half-space of the average resistivity from the potential map. The map of the subtracted potential shows a change from the original data in the south and southeast portion of the map (Figure 9).

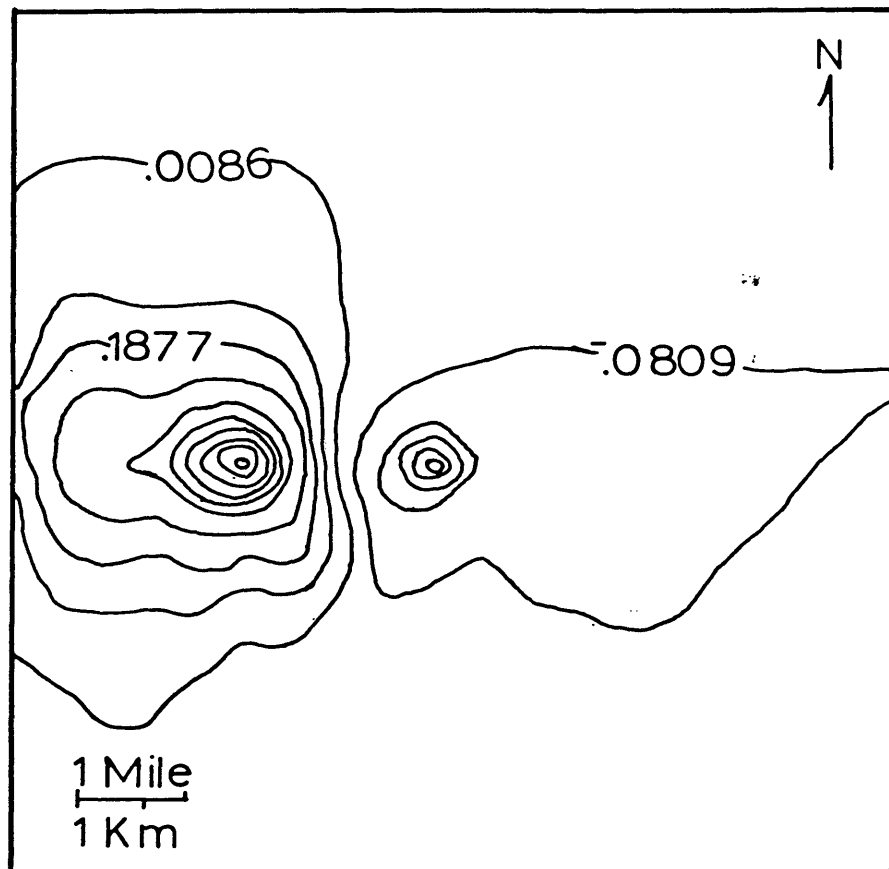
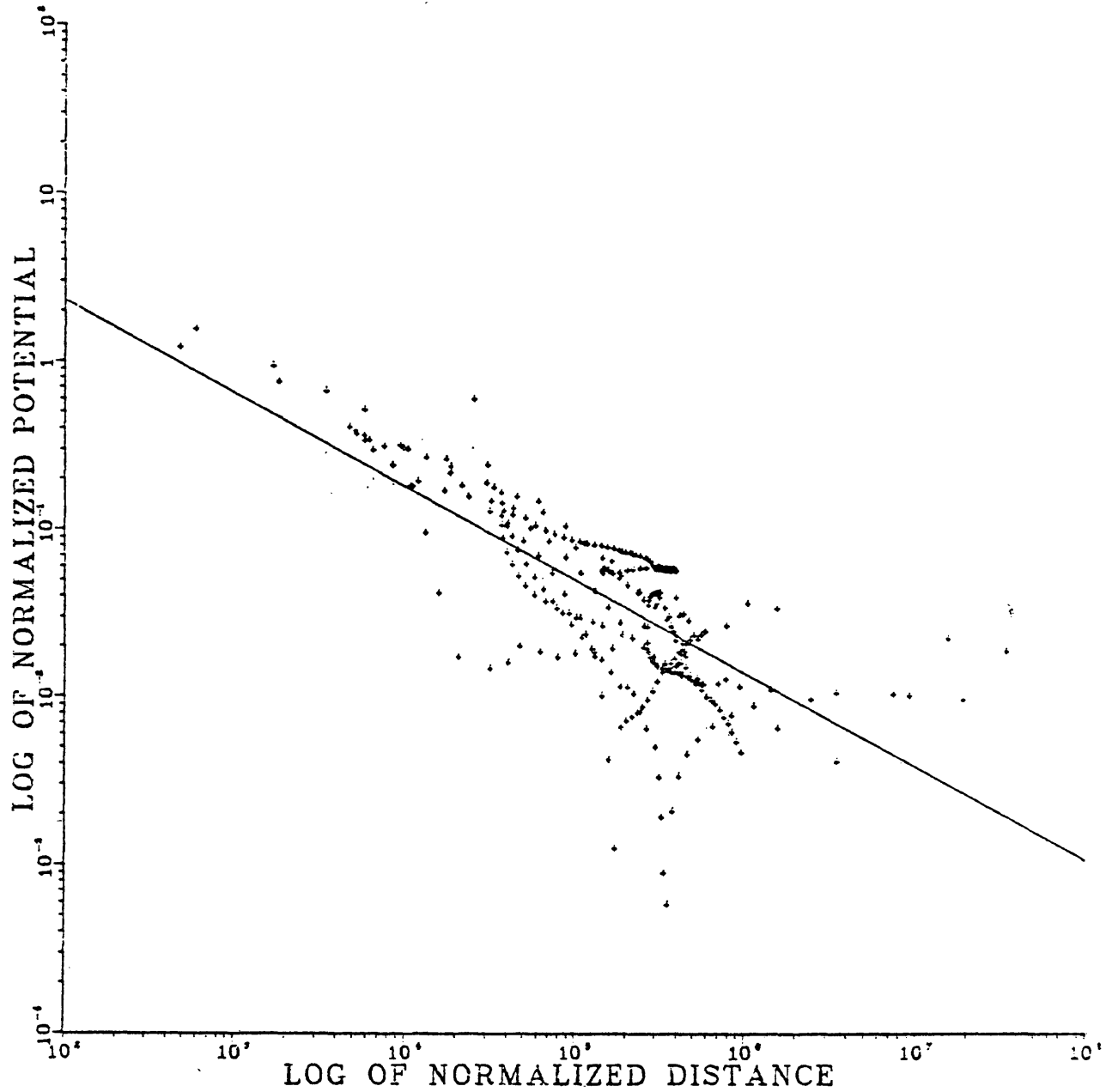


Figure 6. The potential after summation of the potential differences. The contour interval is .0895 volts. The map is of the same area as the base map (Figure 3).

THESIS DATA NORMALIZED BY A FACTOR OF 10,000
AND AN ADDITIVE CONSTANT OF .0118 TO LINEARIZE



$$R_1 / (1 - R_1 / R_2) \text{ (units are 7.8 meters)}$$

Figure 7. Plot of log of potential verses log of normalized distance. It should be noted that the large values of distance are due to the distance used being the geometric factor, which becomes very large when R_1 and R_2 are nearly equal.

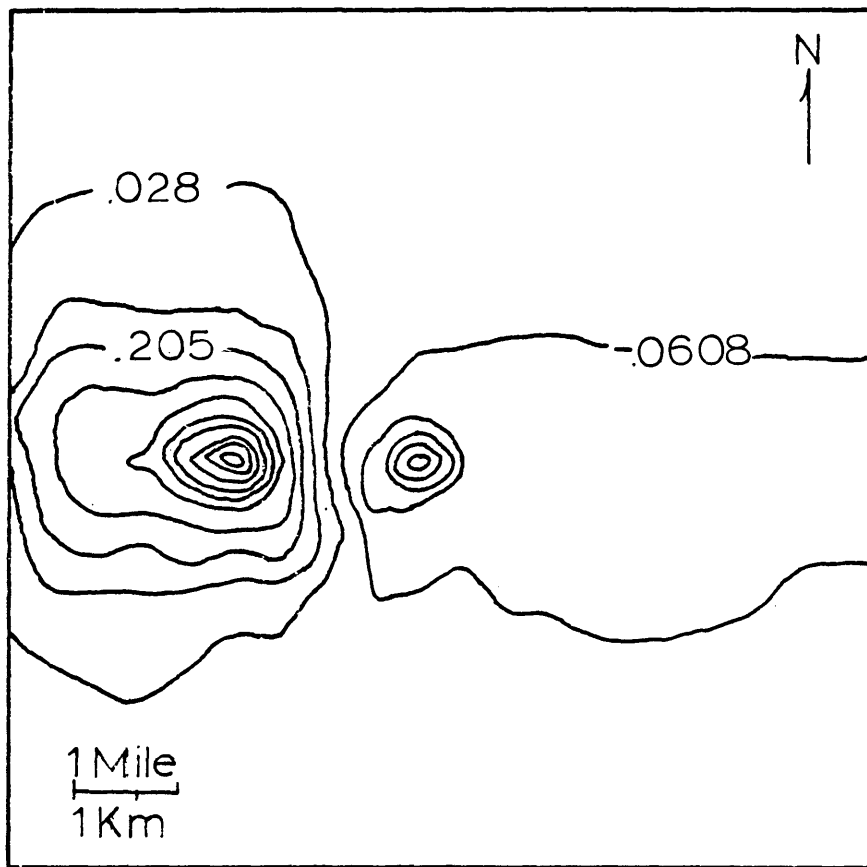


Figure 8. Map of potential with additive constant of 0.0118. The contour interval is .0888 volts. The area of the map is the same as for the base map (Figure 3).

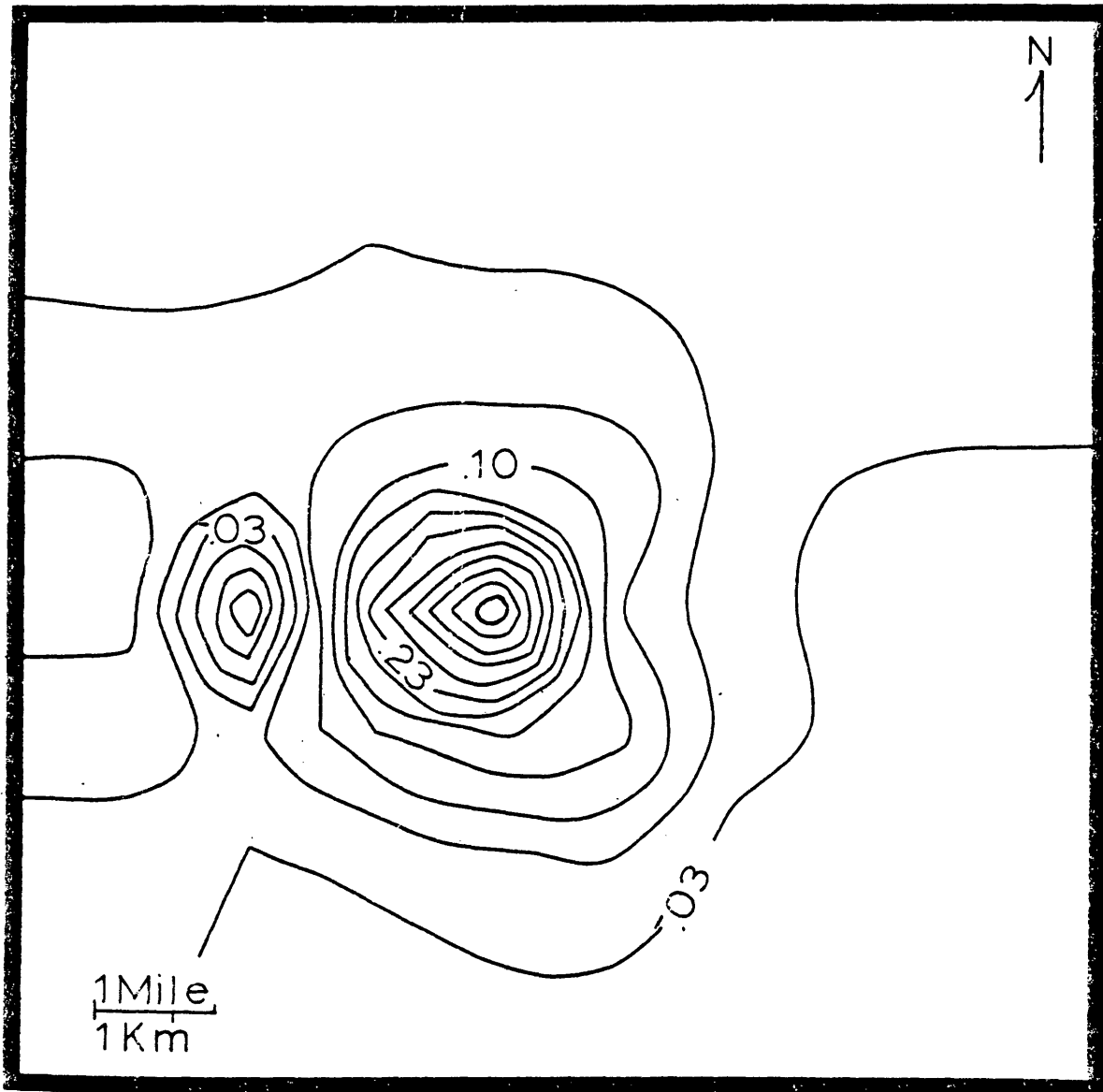


Figure 9. Map of potential after subtracting out a half-space of the average resistivity. The contour interval is .043 volts. The area of the map is the same as for the base map (Figure 3).

RESISTIVITY

Resistivity maps have in the past been the primary interpretive tool used in the dipole prospecting method. The resistivity in this study is rather peculiar since it is found using the potential instead of the electric field. The equation for the resistivity is found by inverting for ρ in equation 5. This gives an equation for resistivity of:

$$\rho = \frac{U 2\pi R_1}{I} (1/(1-(R_1/R_2))) \quad (15)$$

ρ = the resistivity,

U = the potential,

I = the current,

R_1 = the distance from source electrode A,

R_2 = the distance from source electrode B.

The geometric factor:

$$kg = 2\pi R_1 / (1 - (R_1/R_2)) \quad (16)$$

presents several problems (Figure 10). The first problem is that at the center of the source the geometric factor tends to infinity. This is because, at the center of the source, R_1 is equal to R_2 causing the denominator to go to zero. When the geometric factor blows up so does the resistivity, and so those resistivity values are erroneous. To avoid these high values, all resistivities within five degrees of the equator of the source were edited from the

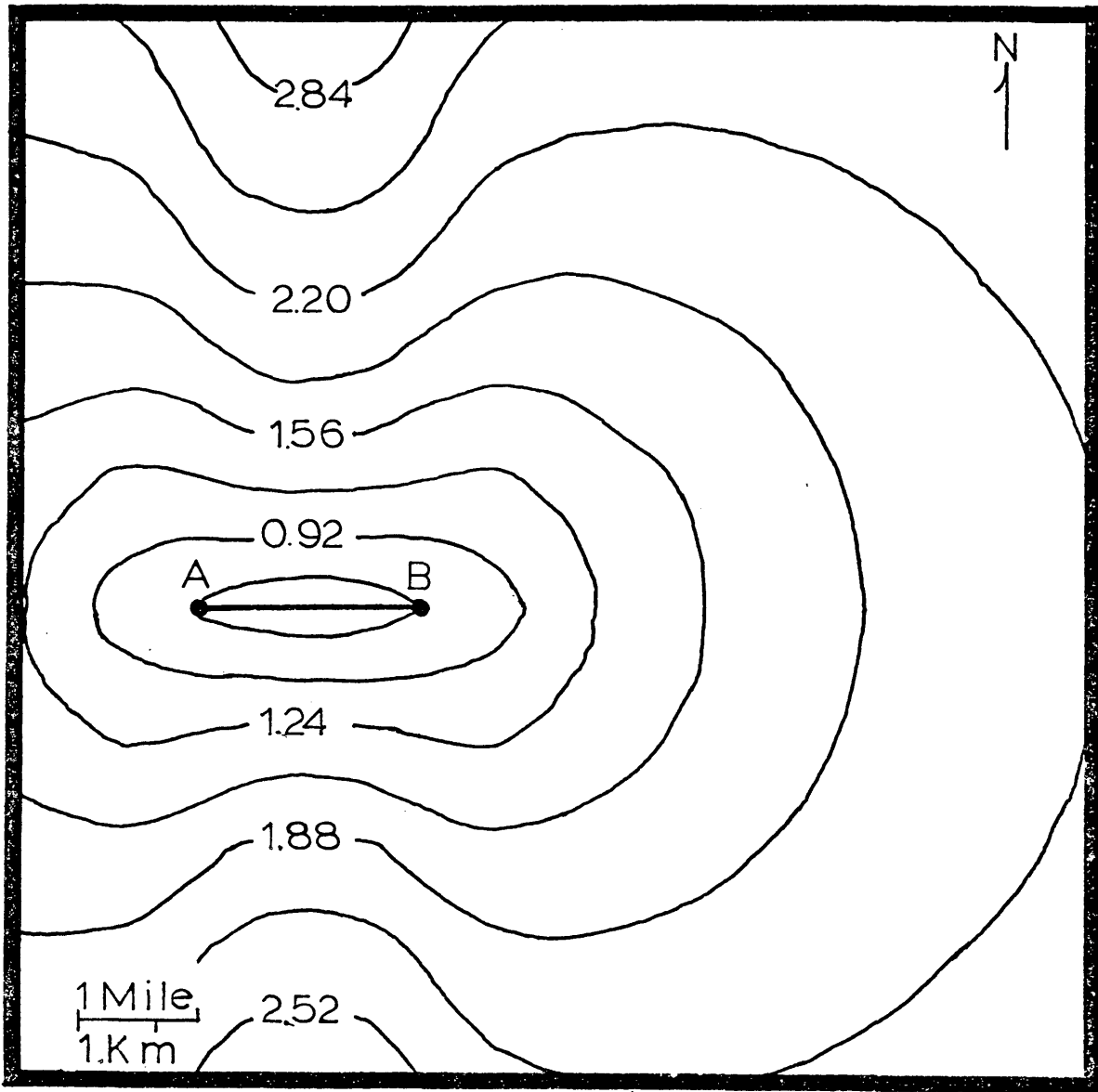


Figure 10. Geometric factor of a bipole source on a half-space of unit resistivity. The contour interval is $10^{0.32}$ meters. The contour values are powers of ten.

resistivity data and map (Figure 11).

The geometric factor or potential may be negative. This sometimes results in negative resistivities. The apparent resistivity map reflects only the absolute value of the resistivity (Figure 12). This map shows a low resistivity area, with values less than 15 ohm-meters, in the center of the map. The southeast corner of the map exhibits high resistivity values. It should be noted that the values on the western part of the map and the northeastern corner are low. These low values are misleading due to a lack of data in these areas. Also, the gridding program, used on this data, smoothed the data causing unreliable values where no data existed.

The apparent resistivity map is consistent with information developed in earlier studies. It is similar to the results of Jordan (1974), Arestad (1977), and Mamah (1979). The high values in the southeast, and the rapid change in values, can not be explained in terms of known geology, and further evaluation is needed.

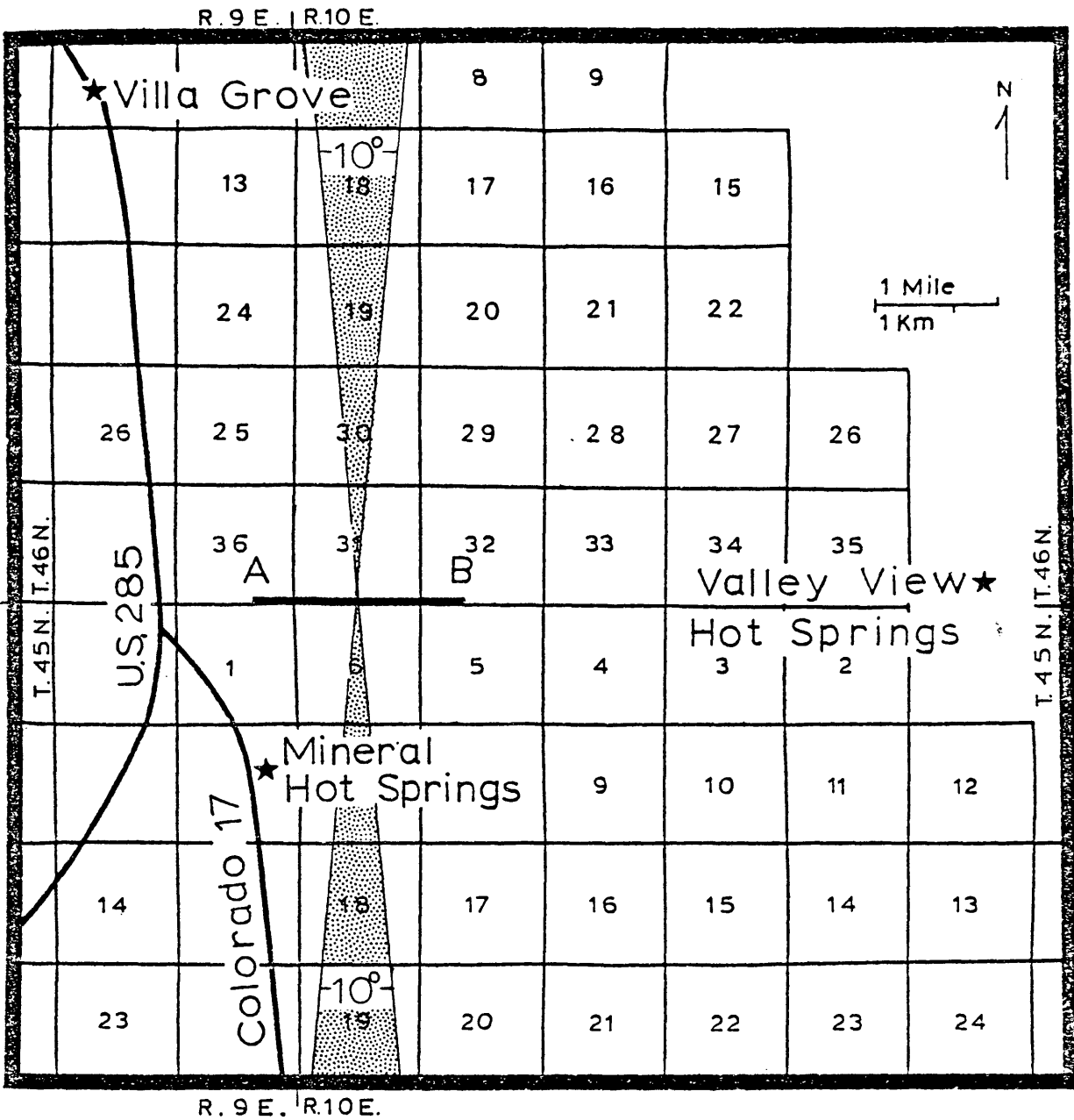


Figure 11. Map of study area showing area in which the resistivities were edited.

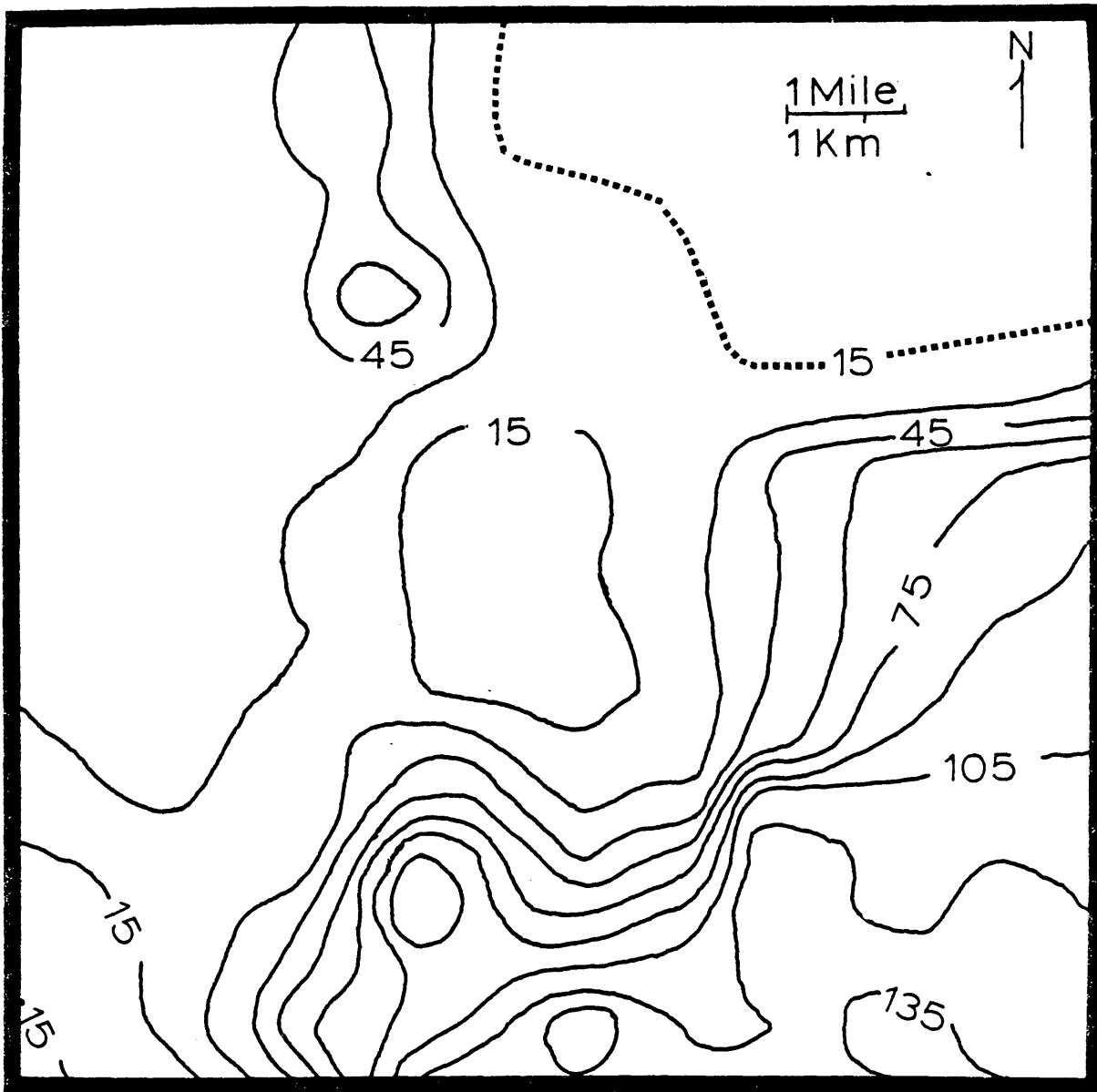


Figure 12. Map of apparent resistivity. The contour interval is 15 ohm-meters. The dashed line is in an area where the quality of the data is in doubt. The map is of the same area as the base map (Figure 3).

SPATIAL FILTERING

Spatial filtering is done primarily to enhance selected wavelengths that are represented in the data. The wavelengths that do not contain the anomaly, and can be considered noise, should be filtered out. For locating the electrical basement of the valley, the long wavelengths are of interest. These long wavelengths carry the information for the broader structures. Also, the effect of the source used can be removed by low-pass filtering, since it is a short wavelength near-surface phenomenon.

There are several methods of spatial filtering that have been developed for use with the potential methods. These methods include high-pass, low-pass, and band-pass filtering (Fuller, 1967; Bhattacharyya, 1976), strike filtering (Fuller, 1967), continuation filtering (Peters, 1949; Dean, 1958; Fuller, 1967; and Bhattacharyya, 1976), and surface fitting (Simpson, 1954; Zurflueh, 1967; and Bhattacharyya, 1969). Downward continuation and surface fitting are the primary methods of filtering that will be used here, but in using these, a combination of low-pass, high-pass, and band-pass filtering will result.

Before any of the filtering techniques were used, it was necessary to get the data into a form that would allow the use of digital filters. This preconditioning of the

data consisted of a gridding of the data on a square grid.

Ideally potential field data should be taken on a gridded pattern in the field. This is not always possible, because of terrain, or in this case, the dendritic pattern which the roads formed. These non-equispaced data need to be put into a gridded form. Many methods of gridding exist, and they include averaging, weighting, fitting to polynomials, and Fourier methods (Crain and Bhattacharyya, 1967).

The averaging methods consist of averaging the values of the data within a certain distance of the grid point. Either simple or geometric averages may be used, with the geometric averaging probably being preferred. A geometric averaging method was tried, and it was found to smooth the data too much. This made it necessary to find a better method of gridding.

The weighting method of gridding is similar to the averaging method, but now the average will be weighted as a function of the distance from the grid point:

$$f(x,y) = \frac{\sum_{i=1}^n w_i(x,y) G_i}{\sum_{i=1}^n w_i(x,y)}, \quad (16)$$

where $w_i(x,y)$ is the weighting function (Crain and Bhattacharyya, 1967). Two weighting functions were tried, linear:

$$w_i = \frac{1}{(x_i^2 + y_i^2)^{\frac{1}{2}}} , \quad (17)$$

and quadratic weighting:

$$w_i = \frac{1}{x_i^2 + y_i^2} , \quad (18)$$

where x_i and y_i are the x and y distance from the grid point to the data point. Test cases showed the quadratic method to be the most satisfactory method, and was used as the method of gridding the data. This method of gridding still smoothed the data, and acted as a low-pass filter. By gridding the data, the shorter wavelengths will be aliased to longer wavelengths, and could add misleading information to the data. In the future, Fourier analysis would add a quantitative approach to seeing how the gridding is smoothing the data, and how the wavelength content is being altered. Also, better methods of gridding, such as polynomial fitting and Fourier methods, would decrease the amount of smoothing of the data.

Now the data are in a form in which we can apply our spatial filters. The data still have the affect of the source and some short wavelength noise that must be filtered out. To take out this unwanted information, the data were fit to low order surfaces. Surface fitting is a method of numerically approximating the data with polynomials. The program used was written by Ronald R. Wahl, special projects

branch of the U.S.G.S., Denver, Colorado. This program, SURFIT, fits orthogonal polynomials to the data using a least squares fit. The program gives out the surface and the residual of that surface. Polynomials as high as nineteenth order can be fit with the program.

The data were gridded on a one mile grid spacing prior to the surface fitting. In Figures 13 through 18, the sixth, eighth, and tenth order surfaces and their residuals are shown.

The sixth order surface (Figure 13) shows a high in the western part of the map. The central part of the map has a north-south trending low. In the eastern part of the map, the values seem to oscillate, and in general are smoothed out. This oscillation and smoothing is due to a lack of field data in these areas.

The residual of the sixth order surface (Figure 14) shows the high and low anomalies due to the source, plus a few high and low oscillations. From the surface and the residual it is seen that the source has been essentially removed from the surface.

The eighth order surface is similar to the sixth, but the high to the west has decreased in size and become elongated in a north-south direction (Figure 15). The central low has been shortened in a north-south direction, and oscillations to the northeast and southeast have become more prominent. The residual map (Figure 16) is similar to the

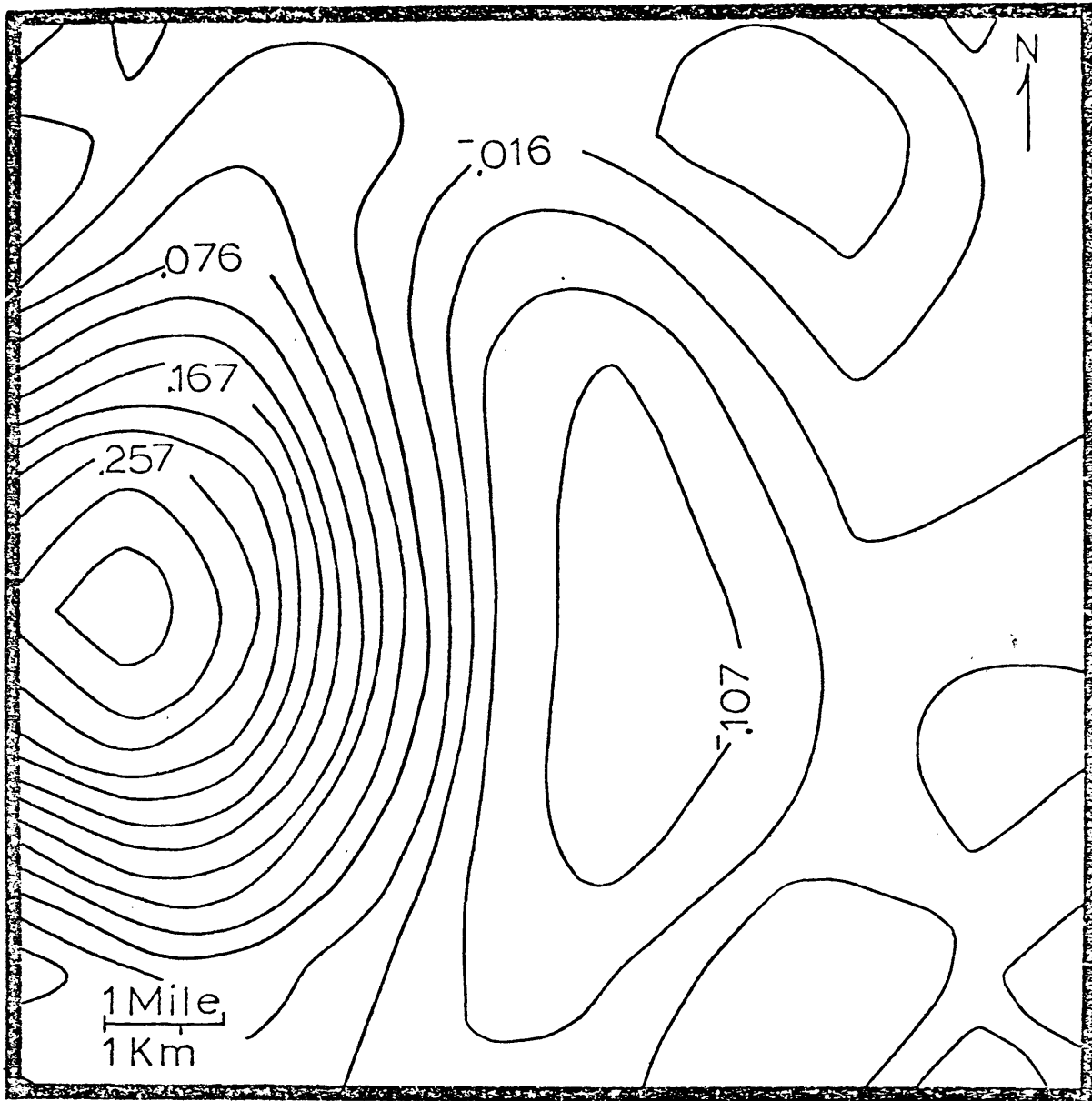


Figure 13. Sixth order surface. The contour interval is 0.0304 volts. The map is of the same area as base map (Figure 3).

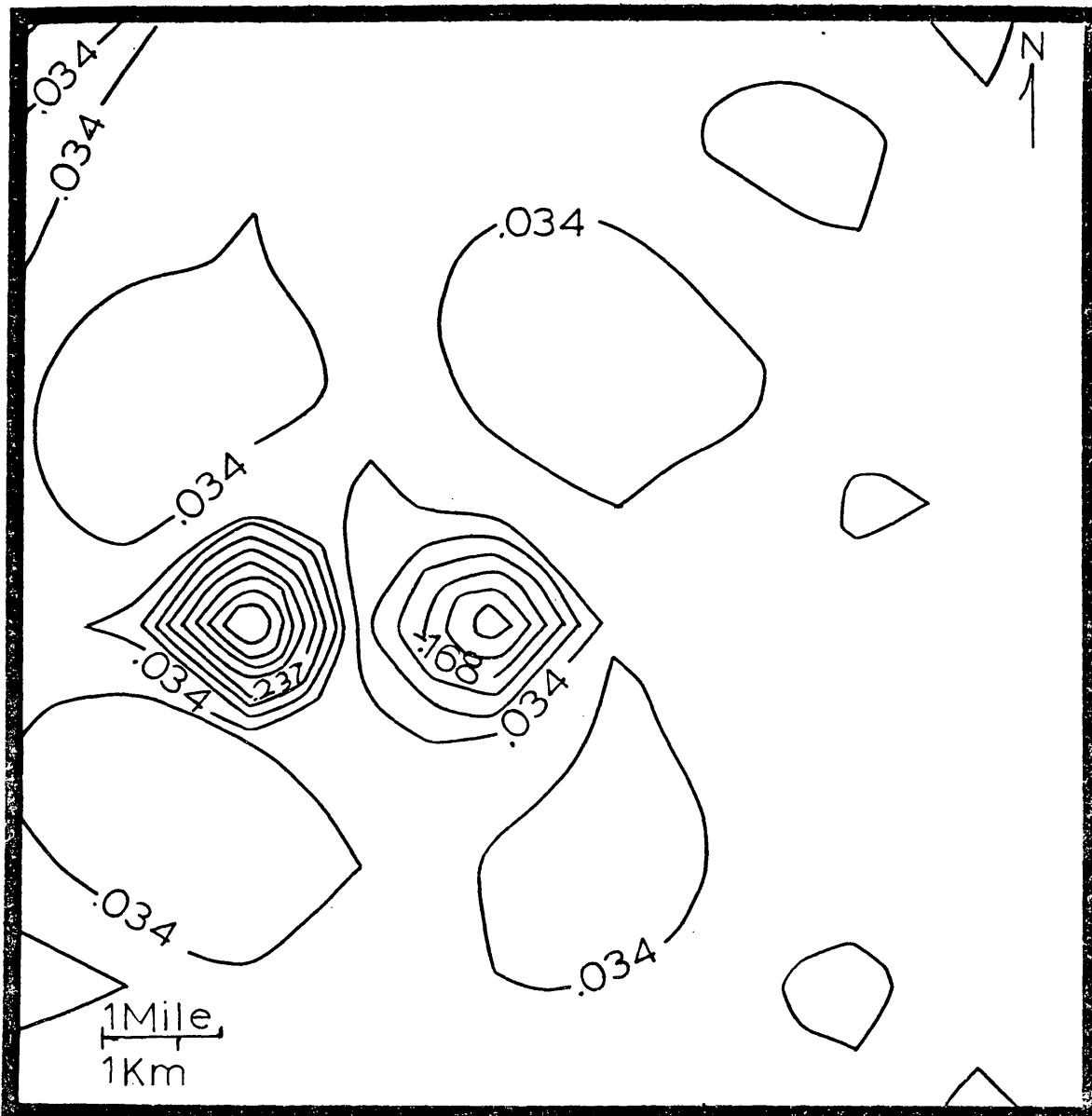


Figure 14. Residual of the sixth order. The contour interval is 0.0675 volts. The map is of the same area as the base map (Figure 3).

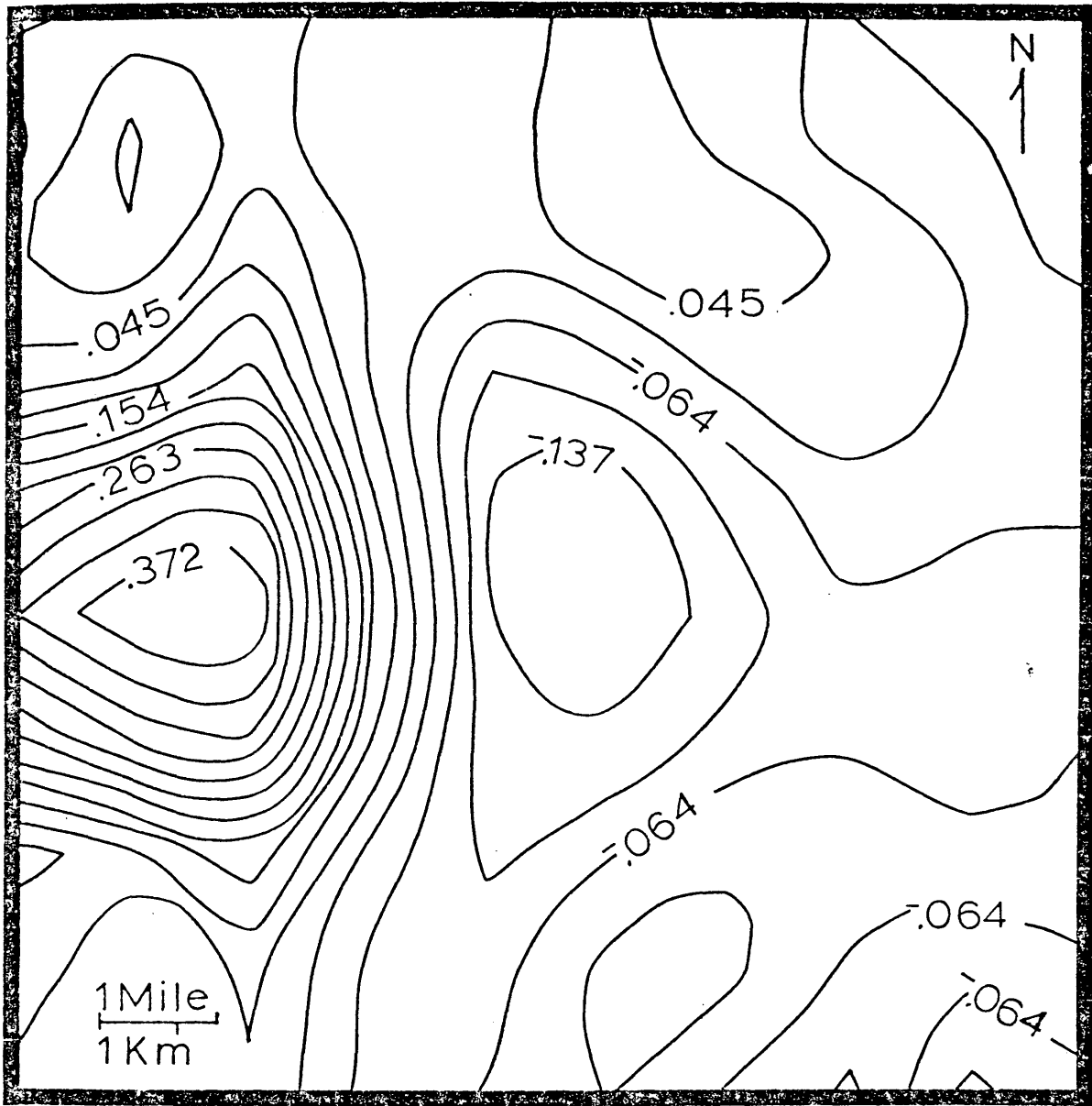


Figure 15 . Eighth order surface. The contour interval is 0.0363 volts. The map is of the same area as the base map (Figure 3).

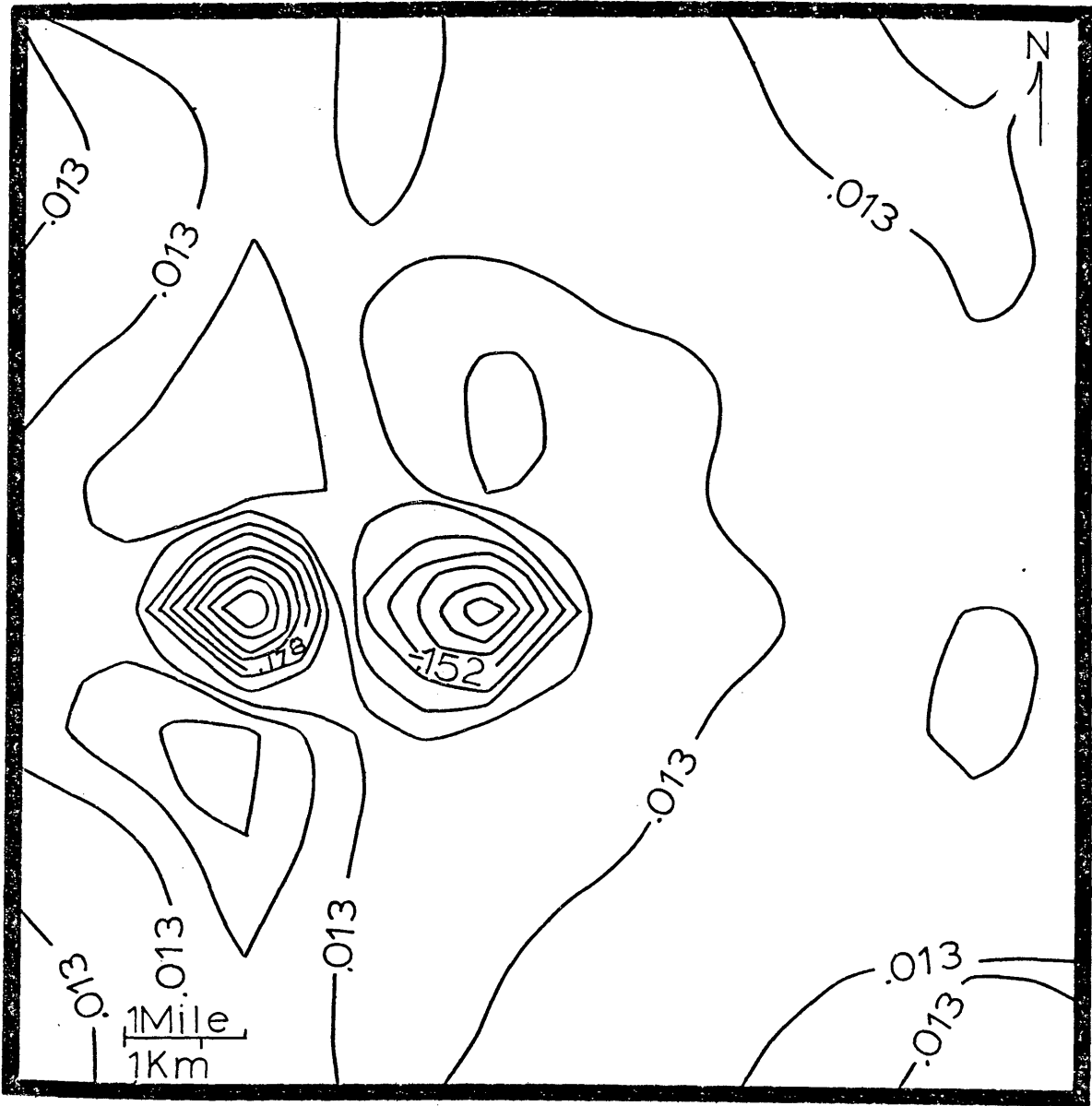


Figure 16. Residual of the eighth order. The contour interval is 0.055 volts. The map is of the same area as the base map (Figure 3).

sixth order residual, but it seems to now have an increased long wavelength content.

In the tenth order surface (Figure 17), the western high has diminished further, and the north-south elongation is further emphasized. The central low is now more or less east-west trending, and the eastern part of the map has lost its oscillatory nature. The surface has taken on more of the appearance of the field data. In Figure 18, the residual looks similar to the surface, except for the high gradient around the central low.

The lower order surfaces represent the longer wavelengths of the data, and by doing so represent the deeper sources or structures, and the larger structures. The high in the western part of the sixth order surface (Figure 13) is in an area where volcanics outcrop, and the central low is coincident with the deepest part of the valley. These two anomalies would then represent an approximation of the valley floor, and so make surface fitting equivalent to an inversion or downward continuation.

To further enhance the data a downward continuation filter was applied to the surfaces. Several filters and developments of the theory of continuation are in the literature (Peters, 1949; Dean, 1958; Fuller, 1967; and Bhattacharyya, 1976). Because of its simplicity, the filter of Peters was used.

The coefficients of Peters (Table 1) are radially sym-

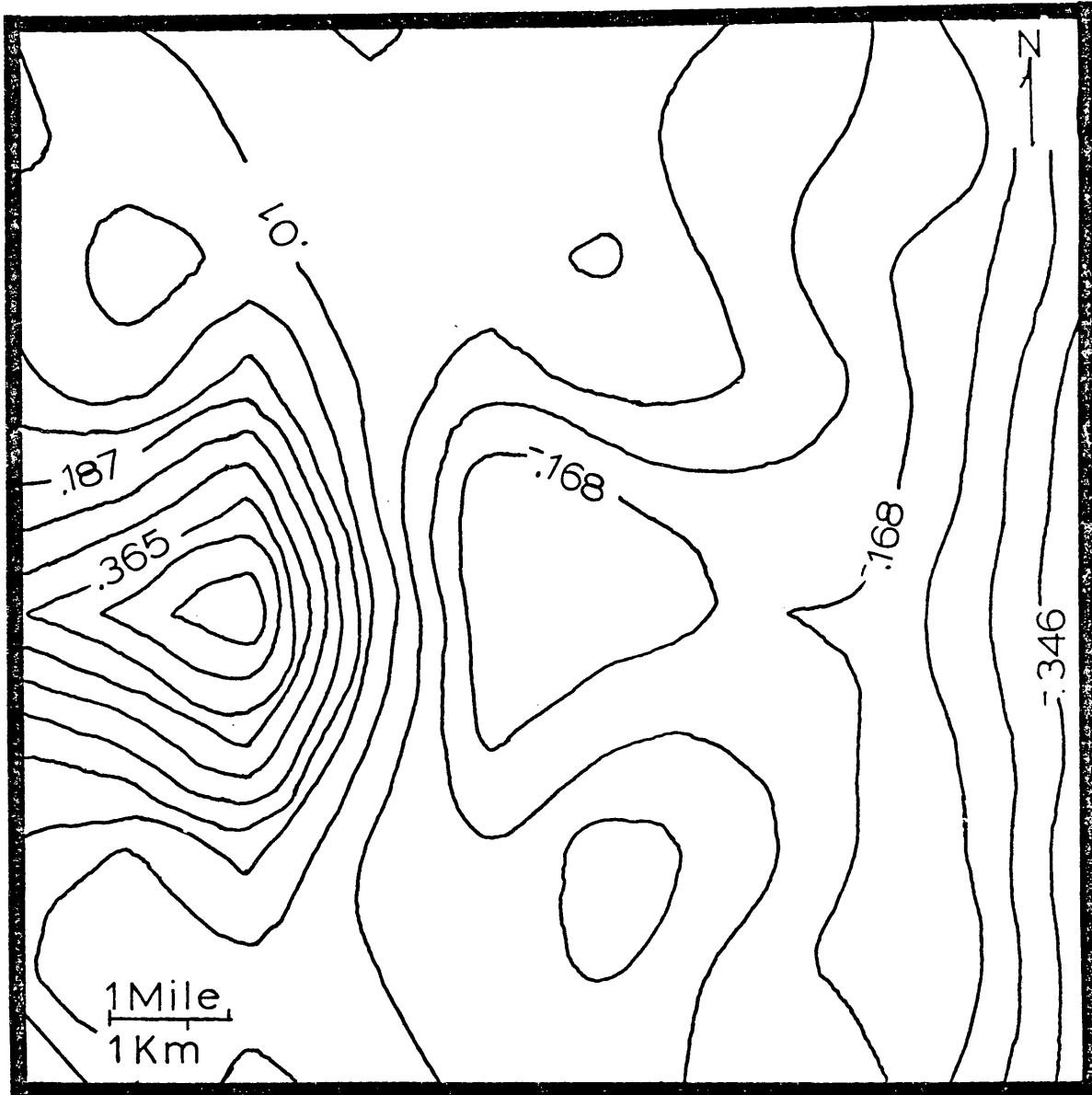


Figure 17. Tenth order surface. The contour interval is 0.0593 volts. The map is of the same area as the base map (Figure 3).

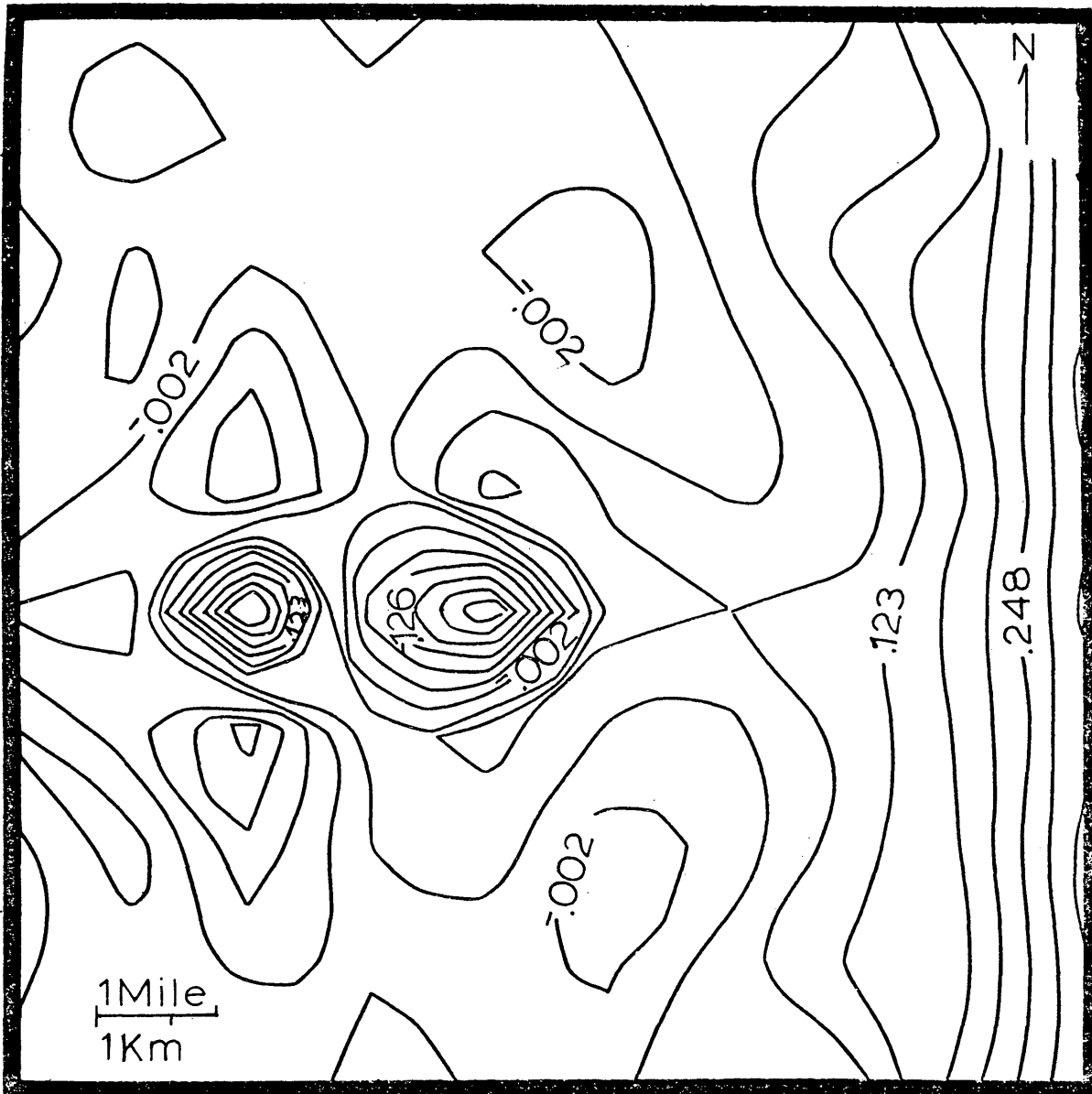


Figure 18. Residual of the tenth order. The contour interval is 0.0415 volts. The map is of the same area as the base map (Figure 3).

Table 1. Filter coefficients used for downward continuation (from Peters, 1949).

circle	depth= 1 coeff.	depth= 2 coeff.
0	.3969	.4197
1	.3026	.3532
2	.3356	.5460
3	.2749	.4071
4	.2234	.2668
5	.0356	-.0442
6	-.2194	-.3762

metric about the point to be continued (Figure 19). Continuation is done by convolving this filter matrix with the matrix of the gridded data. This data set must have a border of fictitious data gridded out around the matrix because data of the width of the filter matrix will be lost in the filtering. This border will keep you from losing any of the real data. The downward continuation should enhance the short wavelength content of the surface.

In Figures 20 and 21 are the sixth order surface continued down one and two grid spacings. The continuation seems to have smoothed the surface, taking out the noise on the eastern part of the map. This filtering enhanced both the high and low anomalies. These two maps have the same appearance, which may suggest that the filters were

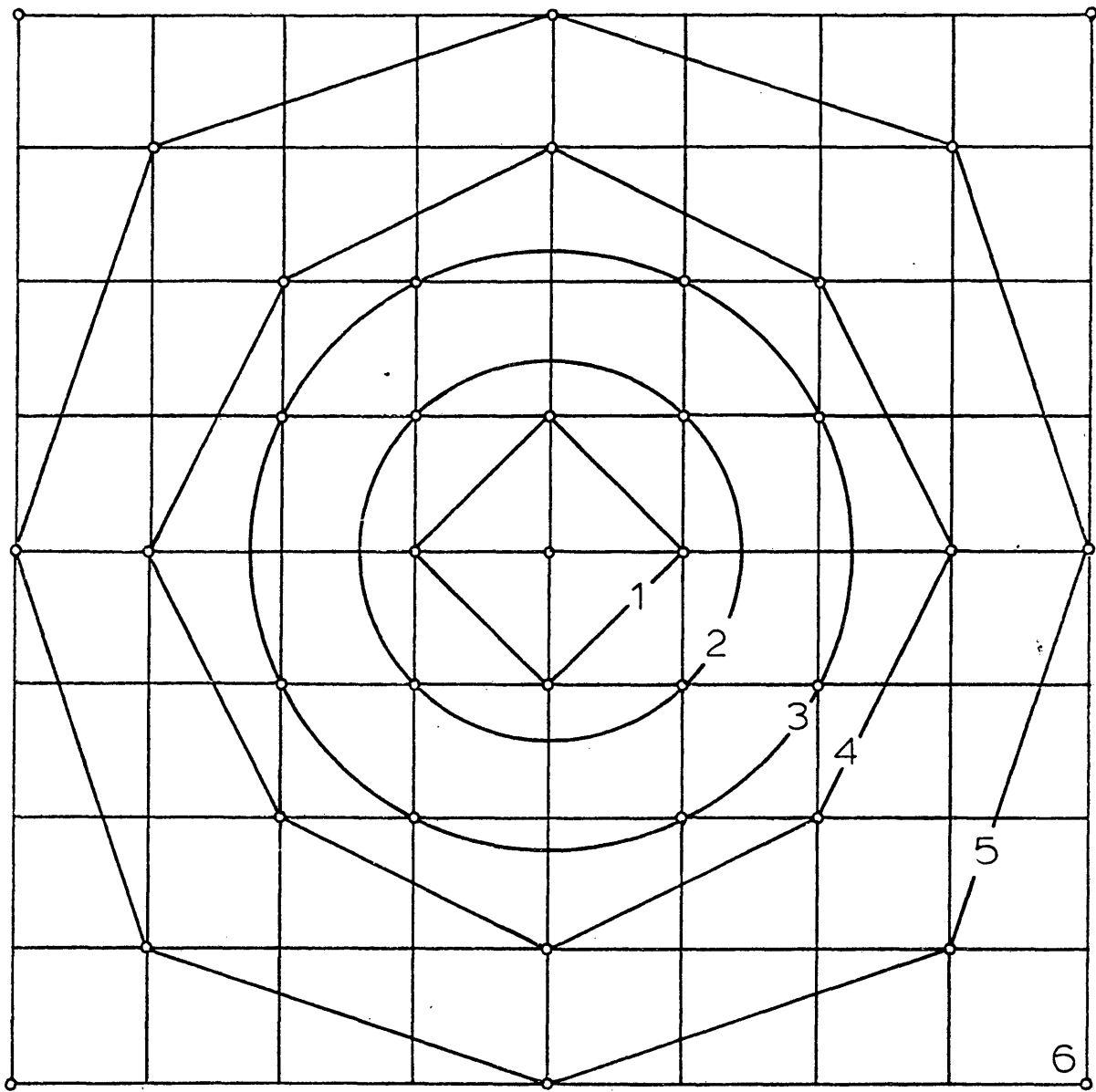


Figure 19. Grid points of the radially symmetric filter.

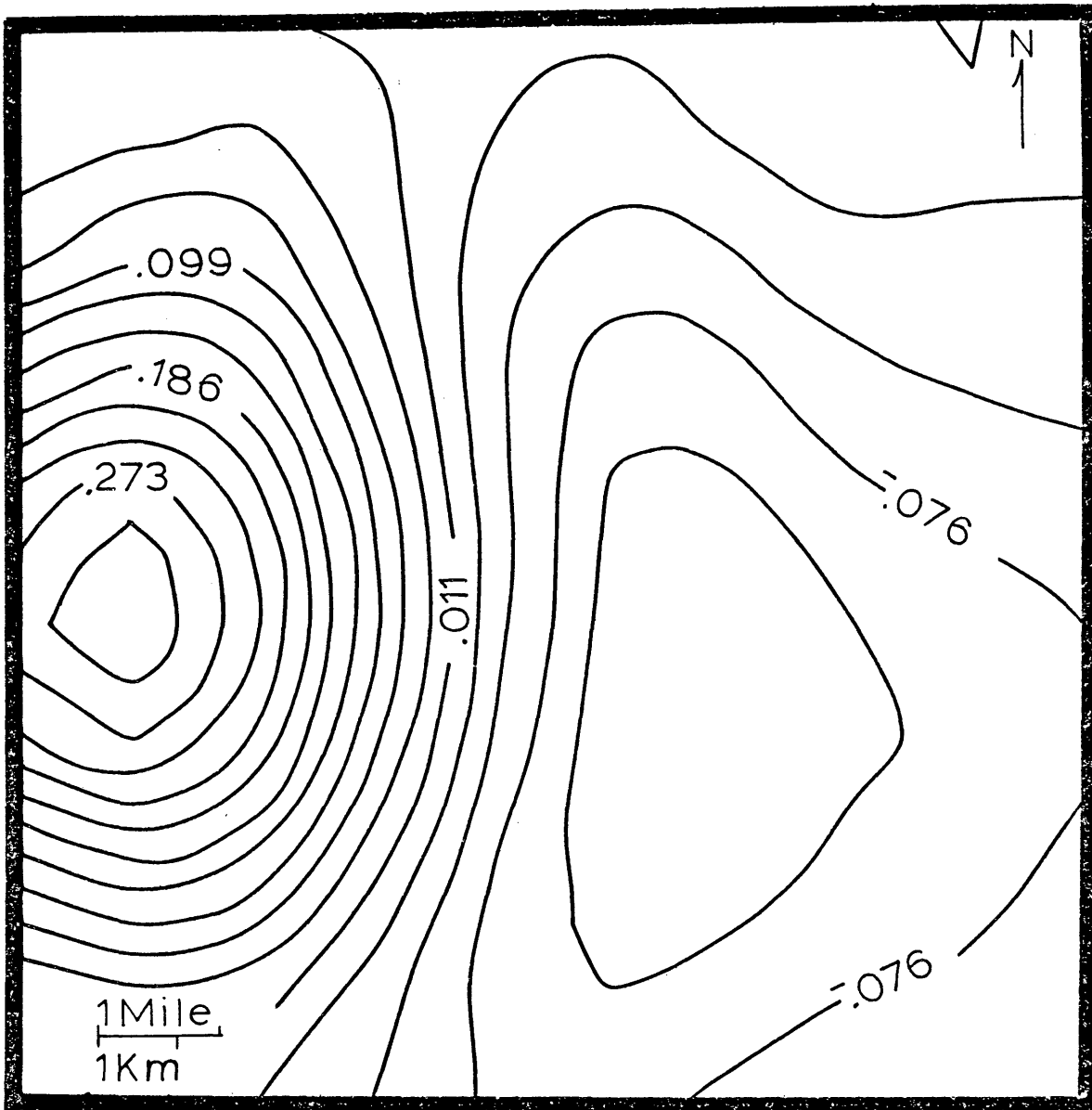


Figure 20. Sixth order surface continued down one mile. The contour interval is 0.0291 volts. The map is of the same area as the base map (Figure 3).

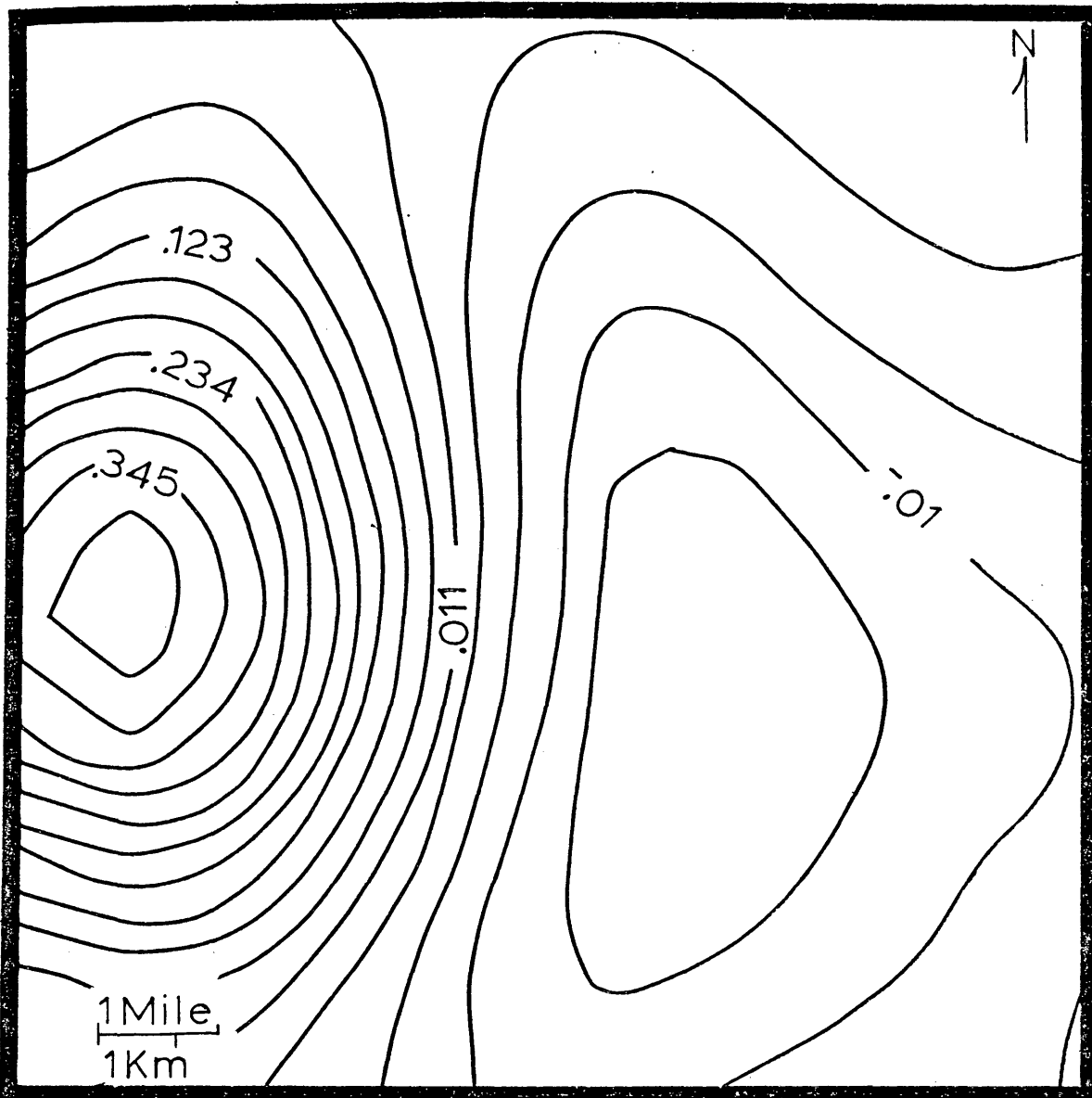


Figure 21. Sixth order surface continued down two miles.
The contour interval is 0.0371 volts. The
map is of the same area as the base map
(Figure 3).

not good enough.

The continuation of the eighth order surface (Figures 22 and 23) tends to filter out the low in the center of the area. This effect is even more prominent in the continuation of the tenth order surface (Figures 24 and 25). The low is totally filtered out making the right half of the map more or less a plane dipping eastwardly. Both the eighth and tenth order continued surfaces have the prominent high in the west. Again, there is little difference between continuation of one grid spacing and two grid spacings.

Continuation has enhanced the anomalies in general, but as higher order surfaces are filtered, there is a tendency to lose the long wavelength anomaly. This is a problem when that anomaly may be of interest. Also, the effect on the wavelength content of the surface fitting and continuation is poorly controlled. Fourier analysis would show the effect of filtering on the data, and thus give better control of the data manipulation and interpretation.

To see smaller structures in the basement rocks it would be necessary to use smaller grid spacings, and band-pass filtering that would separate these wavelengths from the large scale structures, long wavelengths, and the noise, the short wavelengths.

The surface fitting turned out to be roughly equivalent to a continuation, and it effectively removed the source. By continuing the surfaces, the anomalies were generally

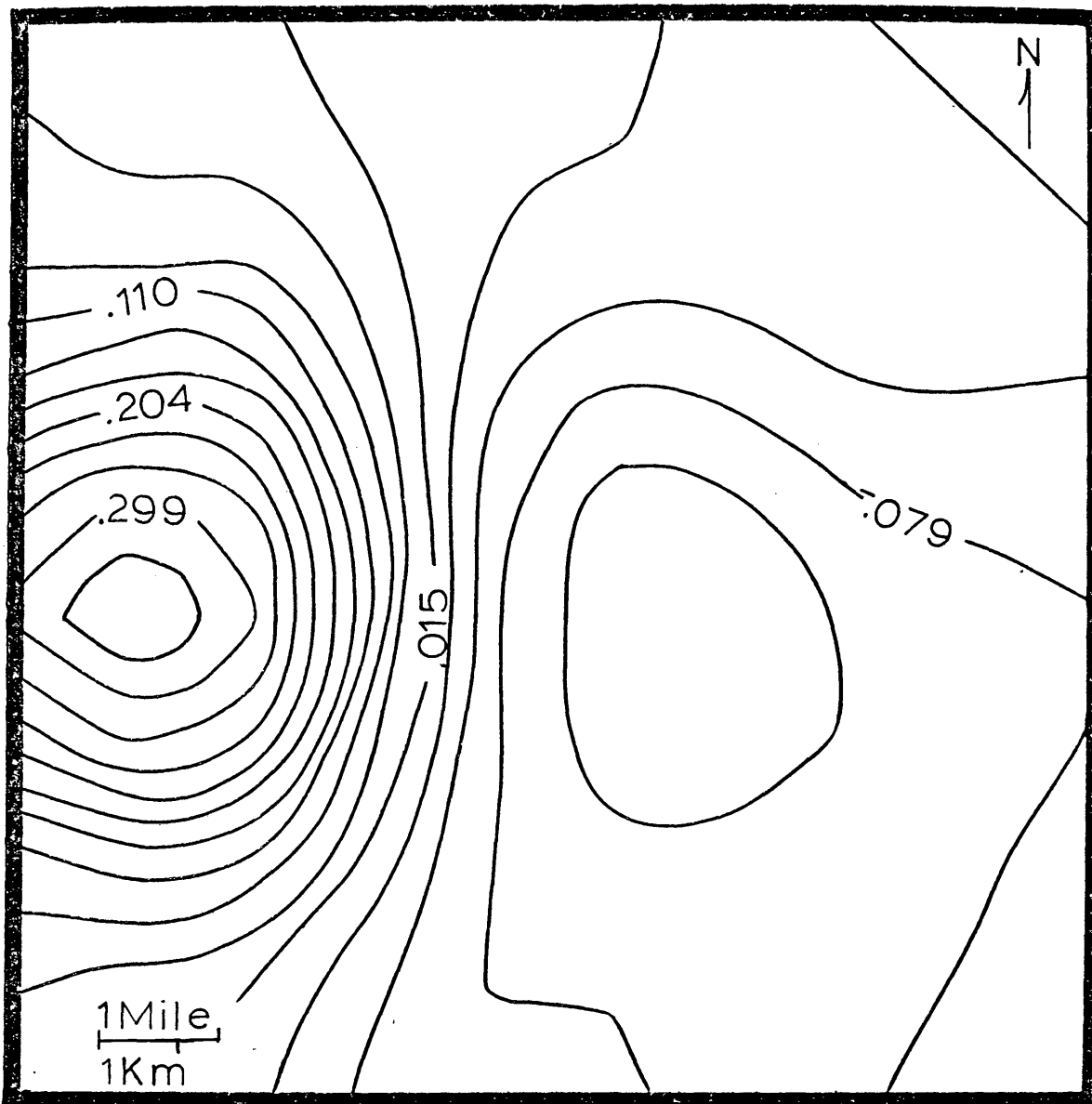


Figure 22. Eighth order surface continued down one mile.
The contour interval is 0.0315 volts. The
map is of the same area as the base map
(Figure 3).

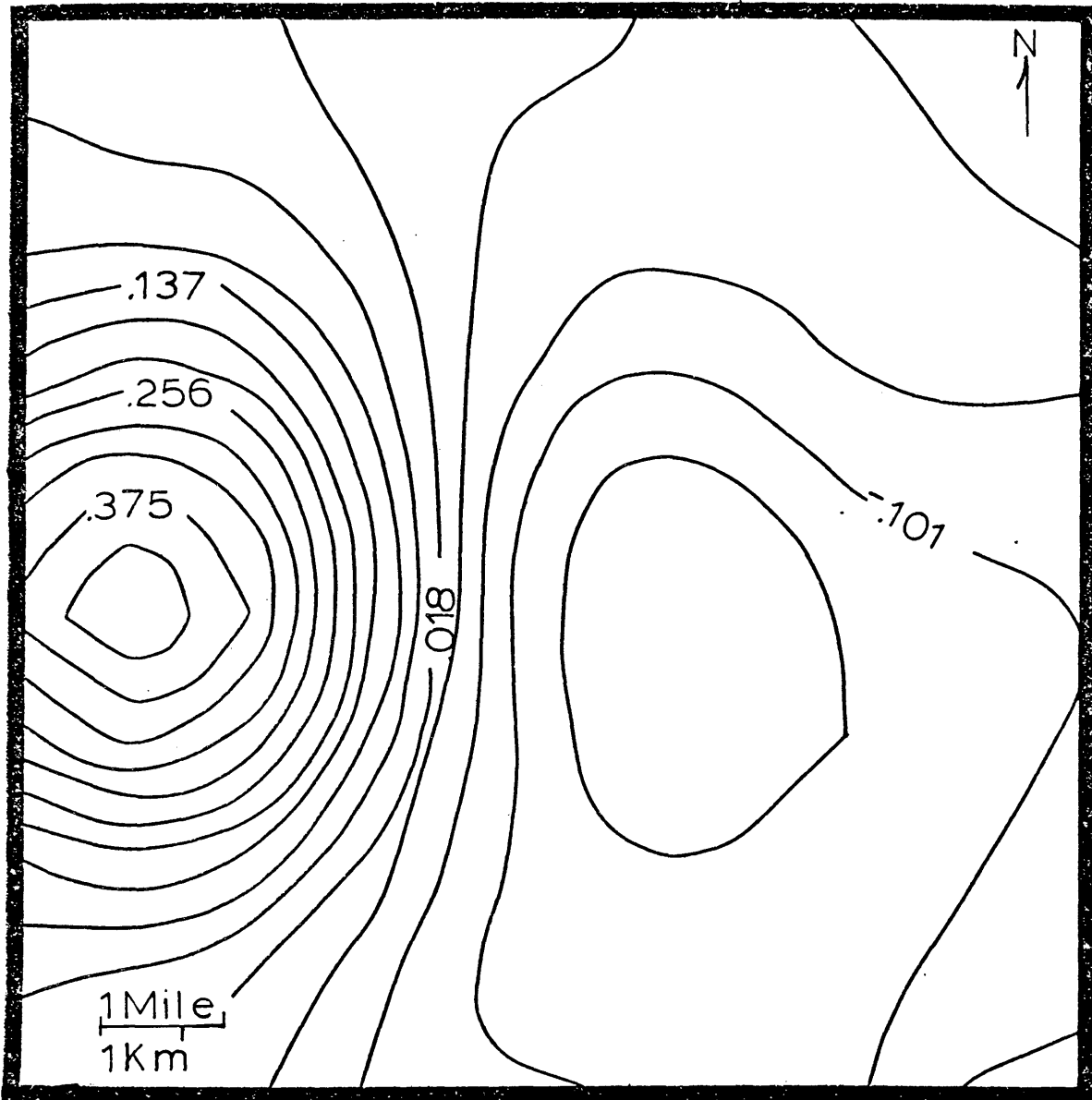


Figure 23. Eighth order surface continued down two miles. The contour interval is 0.0397 volts. The map is of the same area as the base map (Figure 3).

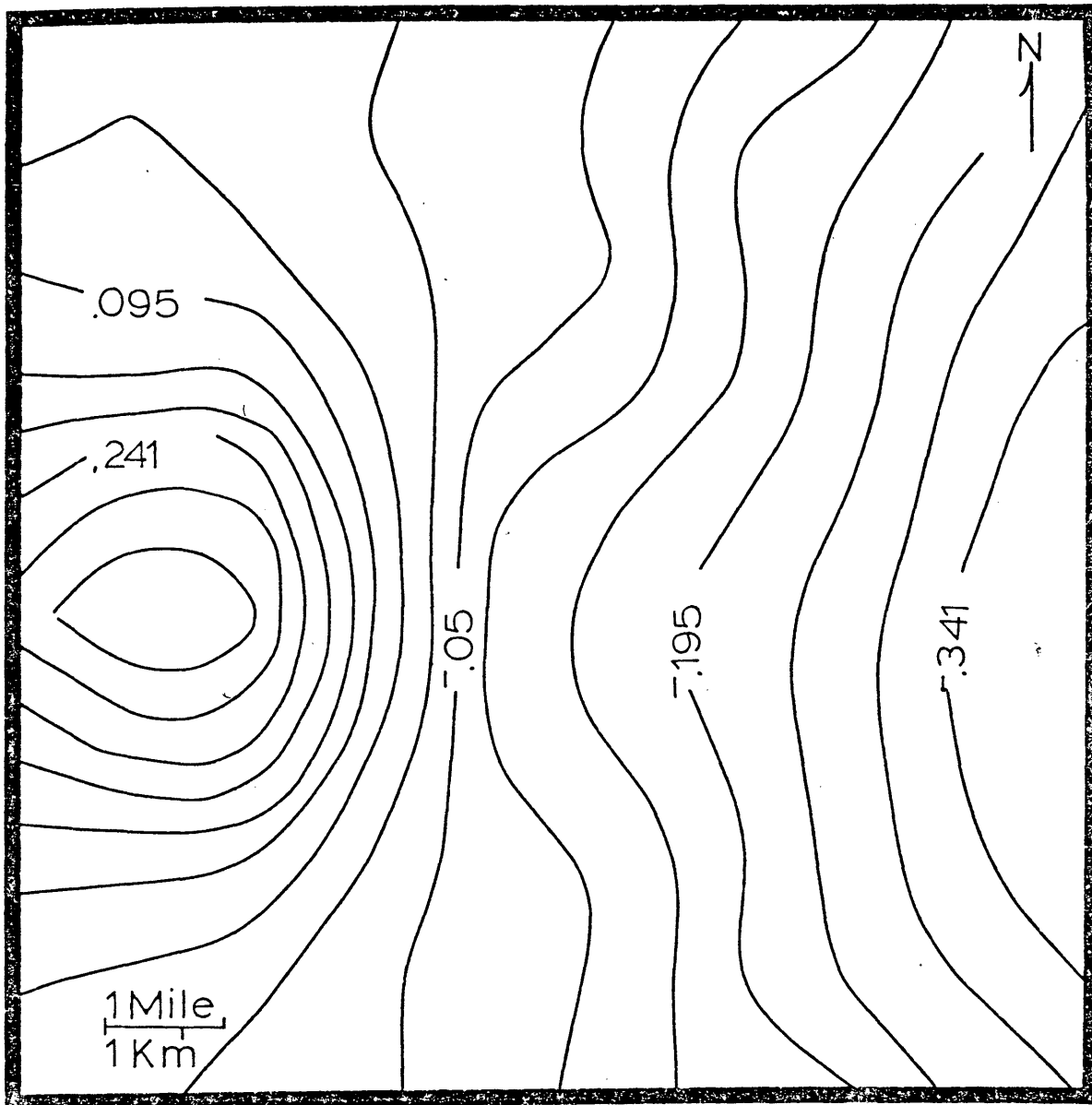


Figure 24 . Tenth order surface continued down one mile.
The contour interval is 0.0485 volts. The
map is of the same area as the base map
(Figure 3).

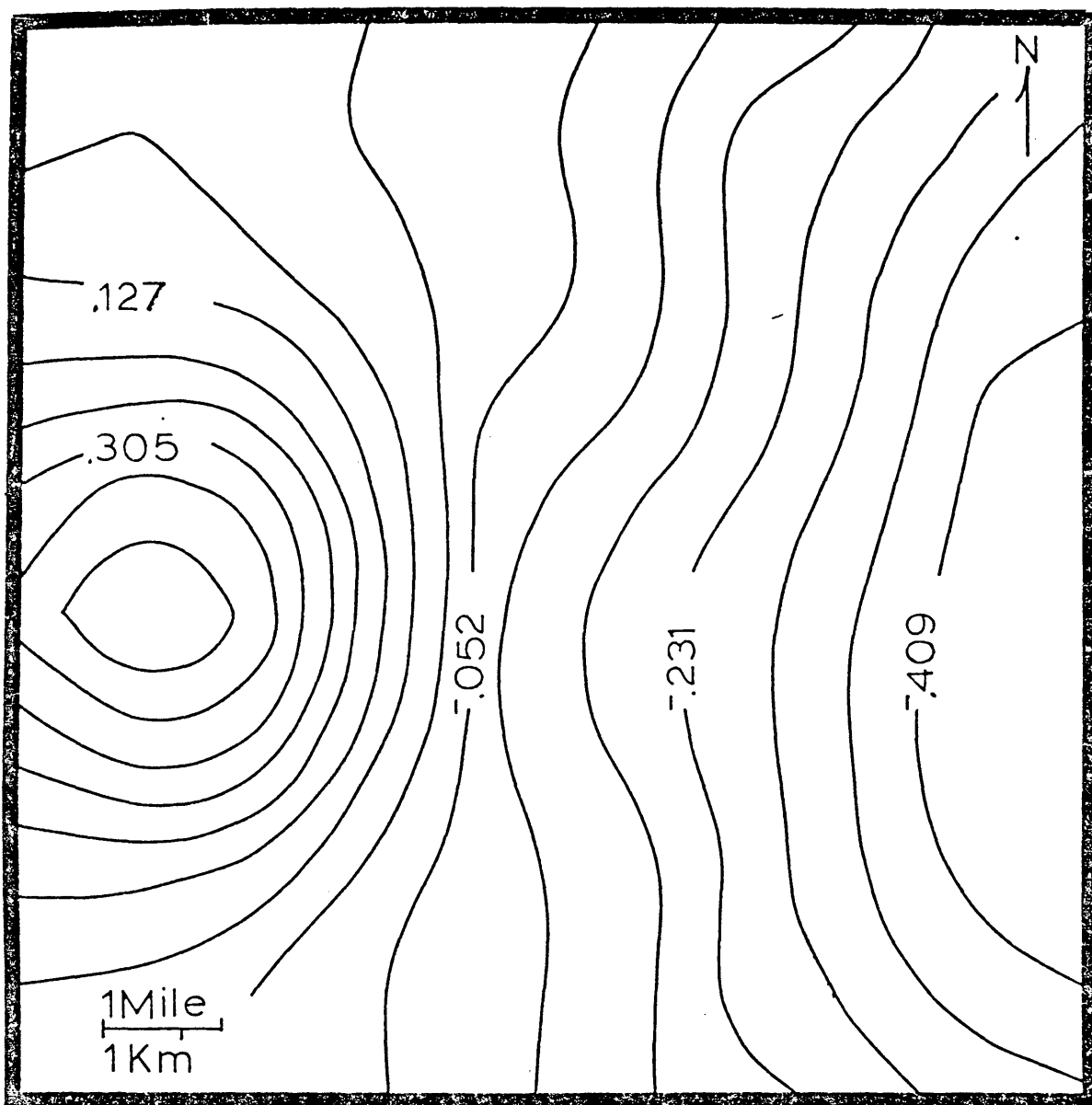


Figure 25. Tenth order surface continued down two miles. The contour interval is 0.0596 volts. The map is of the same area as the base map (Figure 3).

enhanced, but improved filters may increase the usefulness of continuation on this type of data. The surface fitting and continuation were able to delineate the overall structure of the valley floor. The surface fitting removed short wavelengths and the continuation enhanced the short wavelengths. This combination of low-pass and high-pass filtering is equivalent to band-pass filtering.

It may be argued that there physically are no sources in the subsurface to continue the data to. Whether or not the sources physically exist is unimportant, and the filter does not know whether these sources are physical or mathematical. So the filters will enhance the same wavelengths independent of the field or source. This is alright provided you know what you are doing to the wavelength content, and that the anomalies may not be solely due to the field.

Also, there are two primary limitations on continuation. The first limitation is that your filters are not perfect representations of the theoretically derived continuation operator. Secondly, the data can start oscillating due to the enhancement of the high frequencies, and this may be due to noise in the data, or due to continuation through sources which would make continuation invalid since Laplace's equation would no longer hold.

INTERPRETATION

The maps of resistivity and potential give considerable information about the subsurface. Overall, the resistivity map agrees with the trends of the resistivity maps of Jordan (1974), Arestad (1977), and Keller (in Romero and Fawcett, 1978). All four maps have a low down the center of the valley, with high resistivities on the sides of the valley (Figures 26 through 31).

The resistivity map generated in this study (Figure 26) is similar to the apparent resistivity map of Jordan's for the east-west bipole source (Figure 27). Both maps have a central low and high resistivities on the sides of the valley, and in the southern part of the area. Jordan's map also reflects a trend the shape of the valley.

Jordan's map of apparent resistivity due to the north-south bipole source (Figure 28) is considerably different. The low on this map is further north. The central part of the valley has little or no contrast of apparent resistivity as reflected by the near uniform value of 70 ohm-meters.

The apparent resistivities of Arestad's north south bipole (Figure 29) have the central low of this studies apparent resistivity map, but in general Arestad's map is nearly uniform down the center of the valley as is Jordan's map for the north-south bipole. This lack of contrast of resistivity for the north-south oriented bipoles may be due to the bipole being parallel to the valley, and

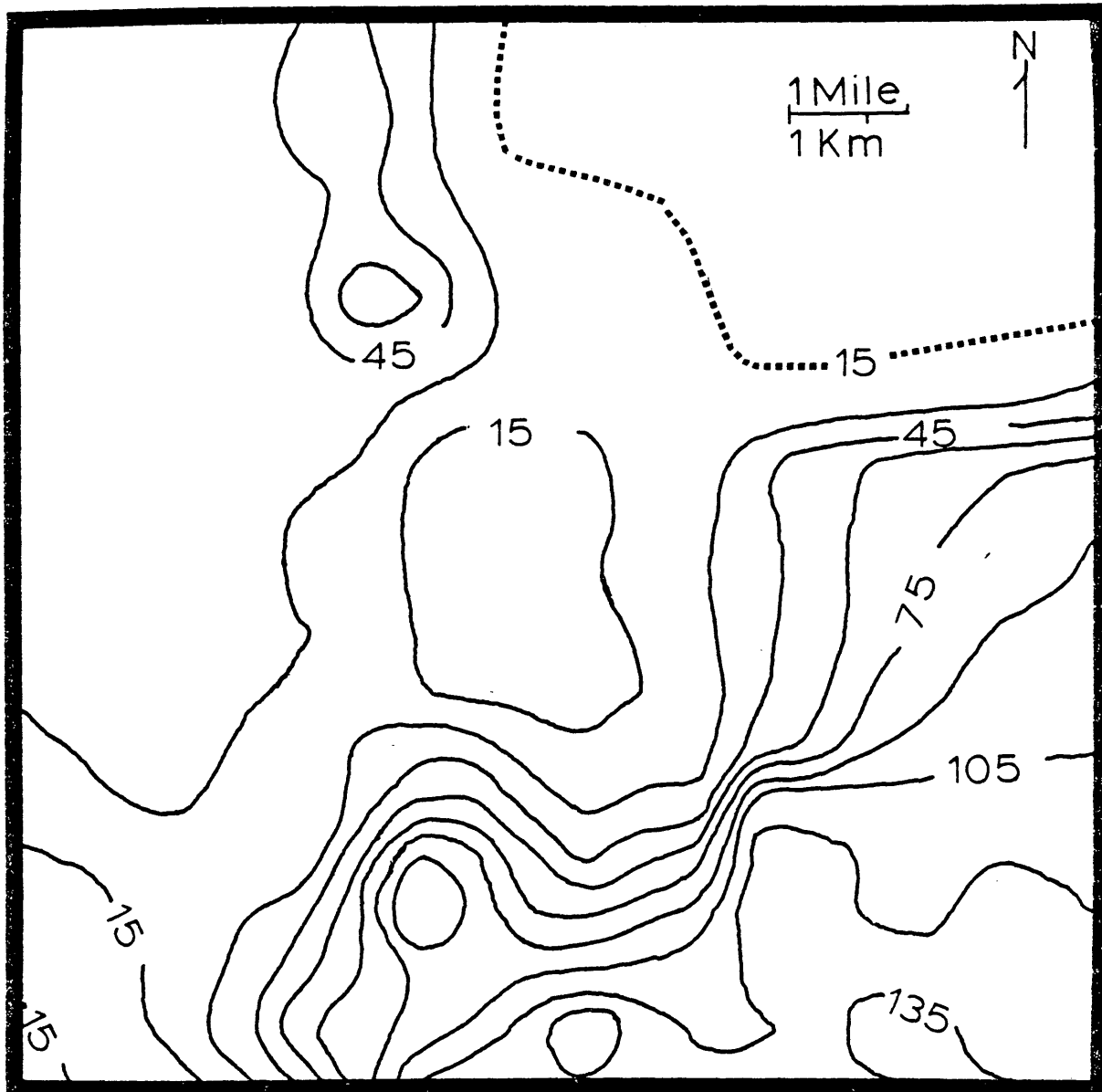


Figure 26. Map of apparent resistivity. The contour interval is 15 ohm-meters. The dashed line is in an area where the quality of the data is in doubt. The map is of the same area as the base map (Figure 3).

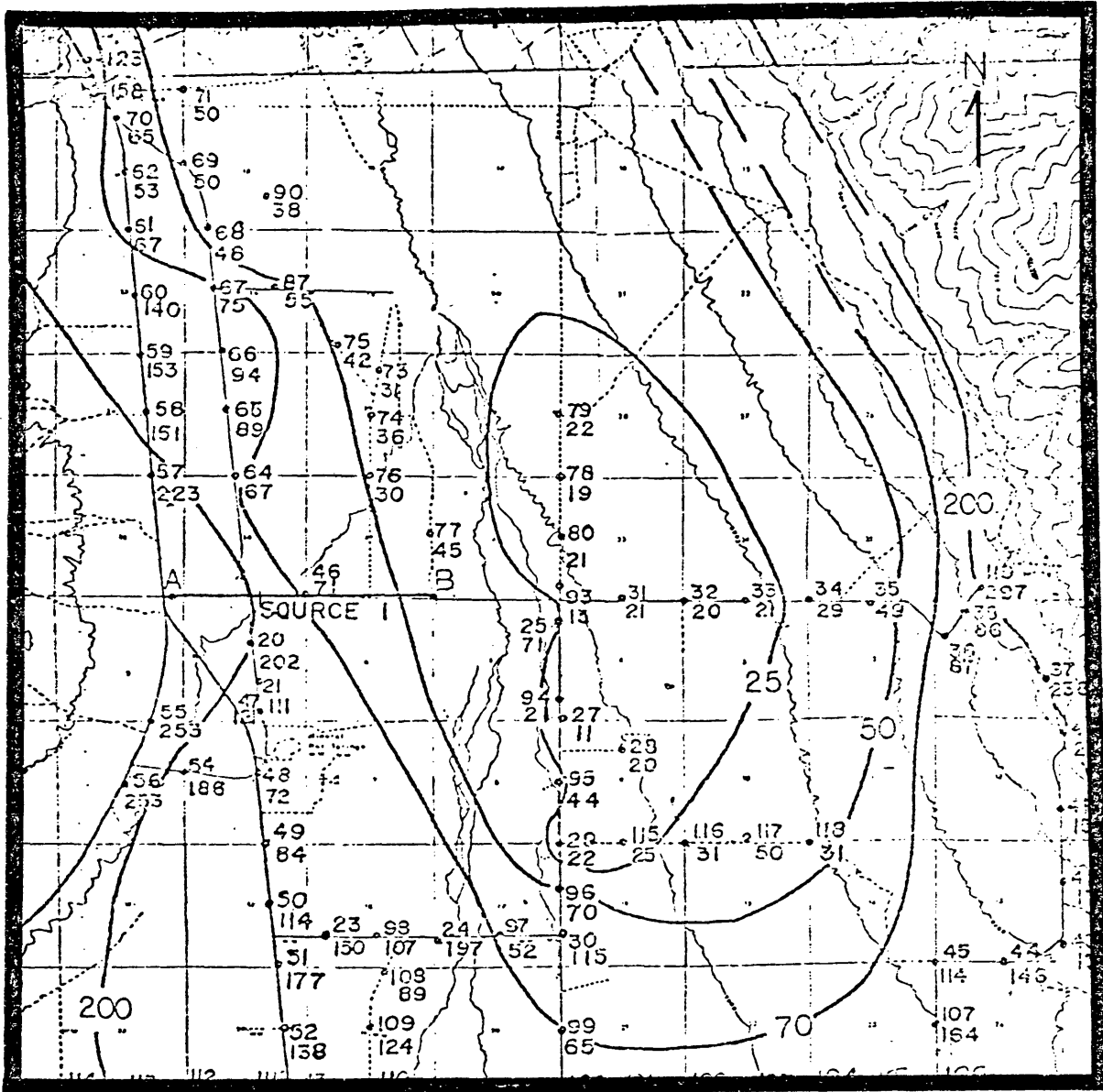


Figure 27. Apparent resistivity map for east-west bipole source (from Jordan, 1974). The contours are in ohm-meters. The map is of the same area as the base map (Figure 3).



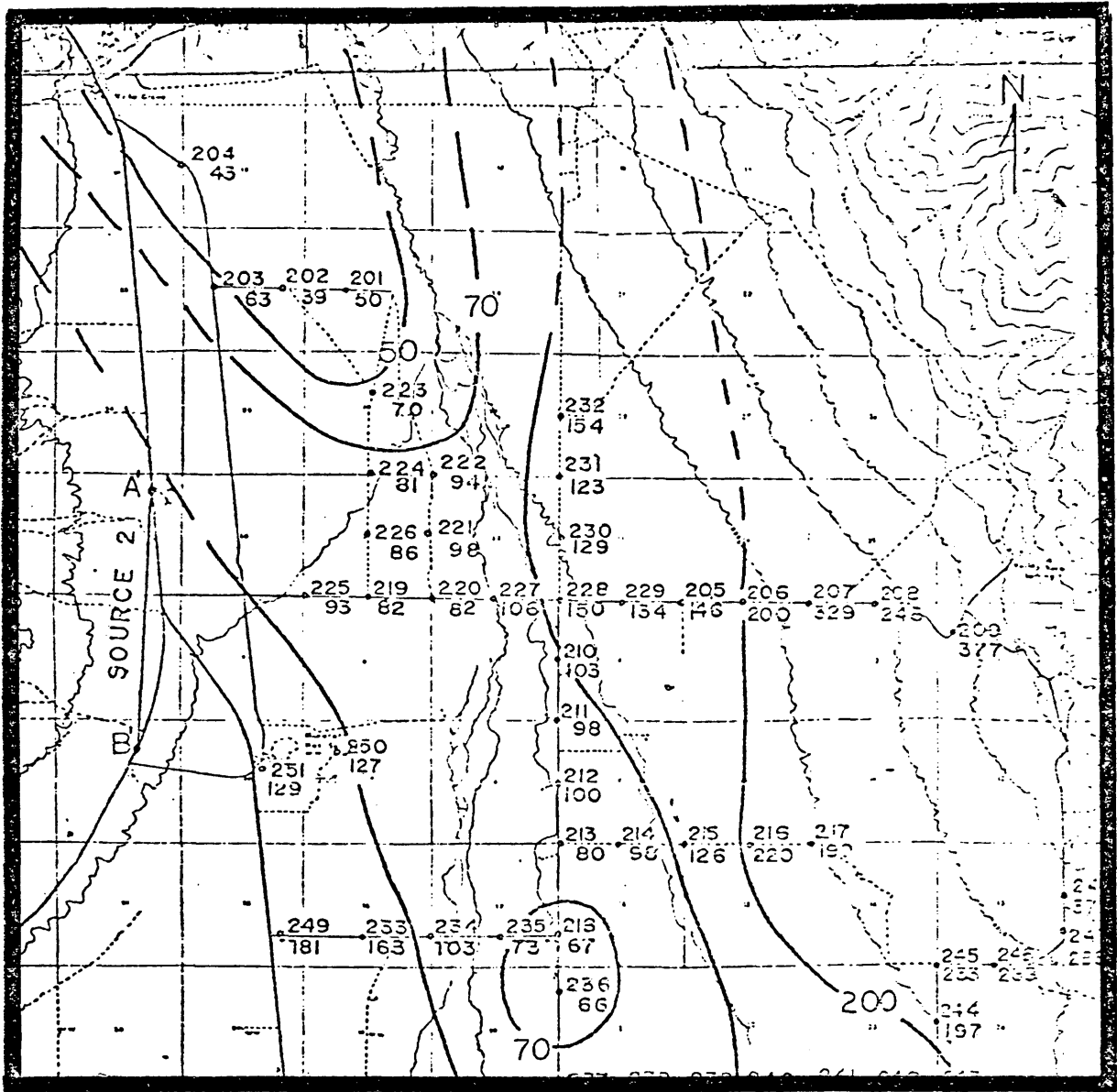


Figure 28. Apparent resistivity map for north-south bipole source (from Jordan, 1974). The contours are in ohm-meters. The map is of the same area as the base map (Figure 3).



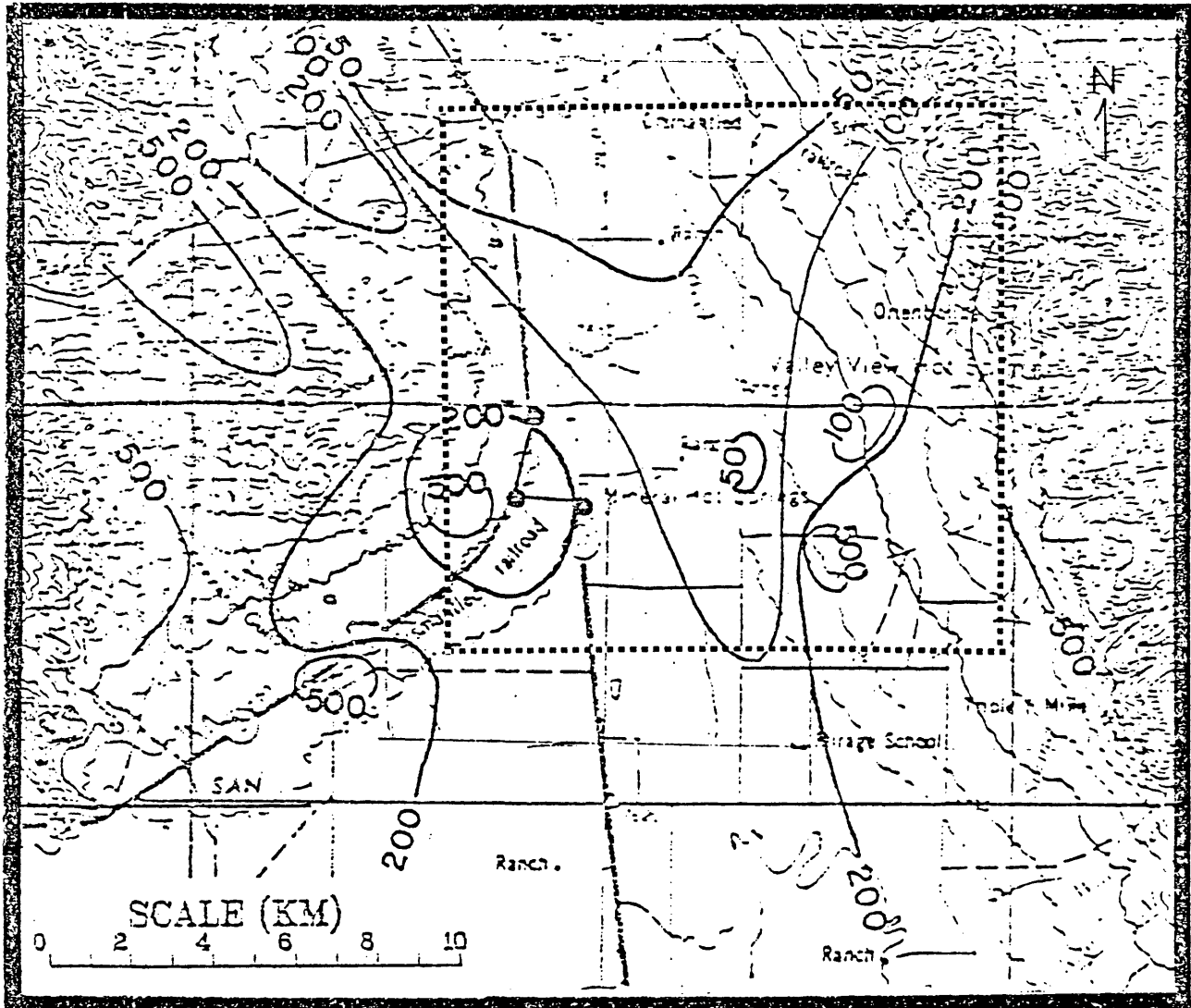


Figure 29 . Apparent resistivity map for the N-S bipole (from Arestad, 1977). The contours are in ohm-meters. The dashed area is the same area as the base map (Figure 3).

that the resistivities due to this orientation may only be showing the effect of a half-space over the central part of the valley.

Again, there are similar features to the apparent resistivity map of this study and that of Arestad's apparent resistivity map for an east-west bipole (Figure 30). There is a closed low area in Arestad's map, with high values to the south and to the sides of the valley. But, the lows tend to not be over the middle of the valley as in the map of this study.

Probably, the best comparison can be made with the apparent resistivity map of Keller (Figure 31). This map has a central low and a gradient of apparent resistivity going to higher values to the south. On both Keller's map and the apparent resistivity map of this study, the gradient in resistivity to the south can not currently be explained.

The filtered potential map gives considerable information about the basement structure (Figure 32). In the west, the high corresponds to volcanics that outcrop further west, and so shows the subsurface extent of these volcanics. The low corresponds to the deepest part of the valley as shown by Jordan (Figures 33 and 34), Stoughton (1977), and Romero and Fawcett (Figure 35). Also, the low corresponds surprisingly well with the 25 ohm-meter contour of Jordan's resistivity map (Figure 27). A crosssection of

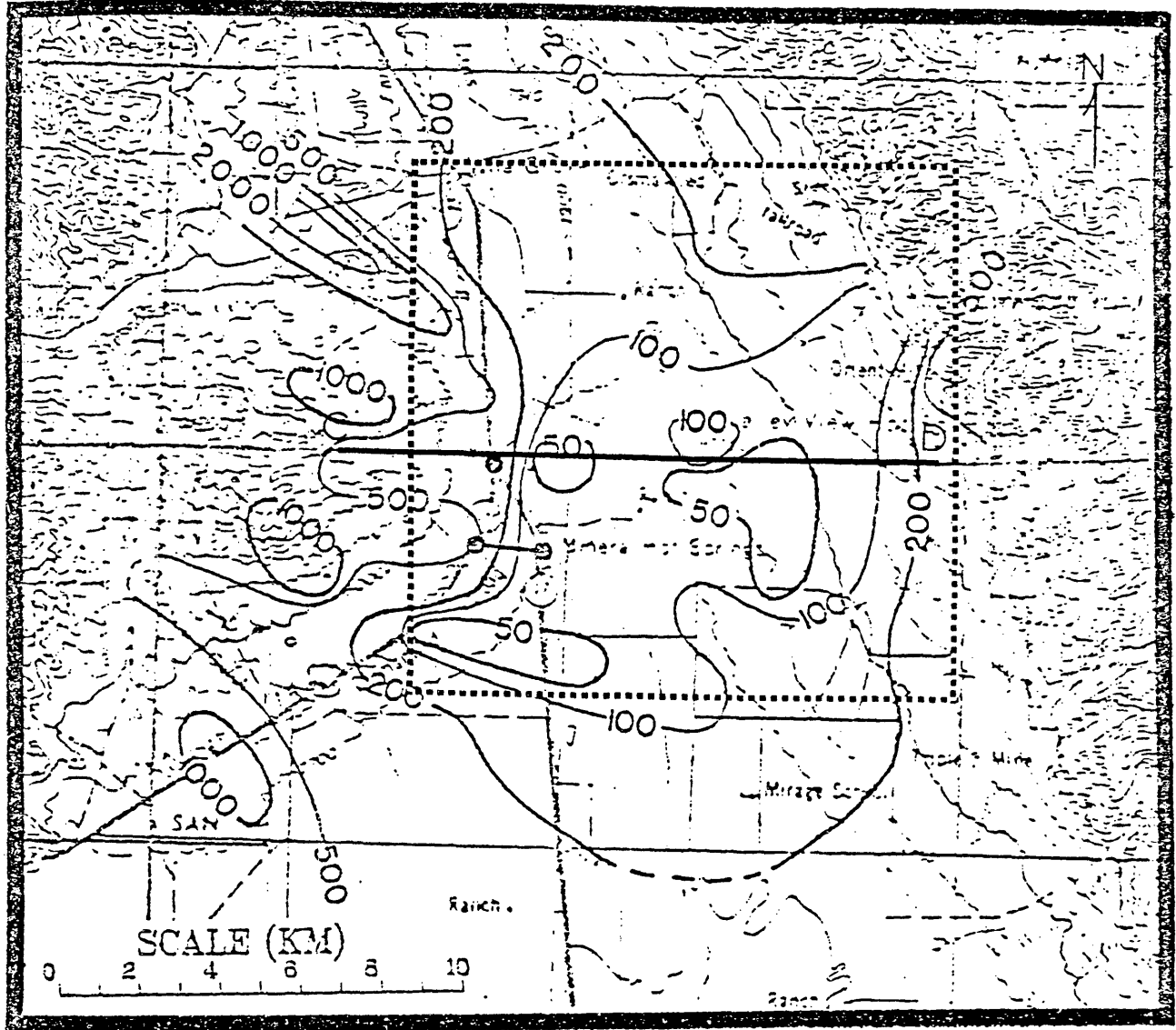


Figure 30. Apparent resistivities for E-W bipole source (from Arestad, 1977). The contours are in ohm-meters. The dashed area is the same area as the base map (Figure 3).

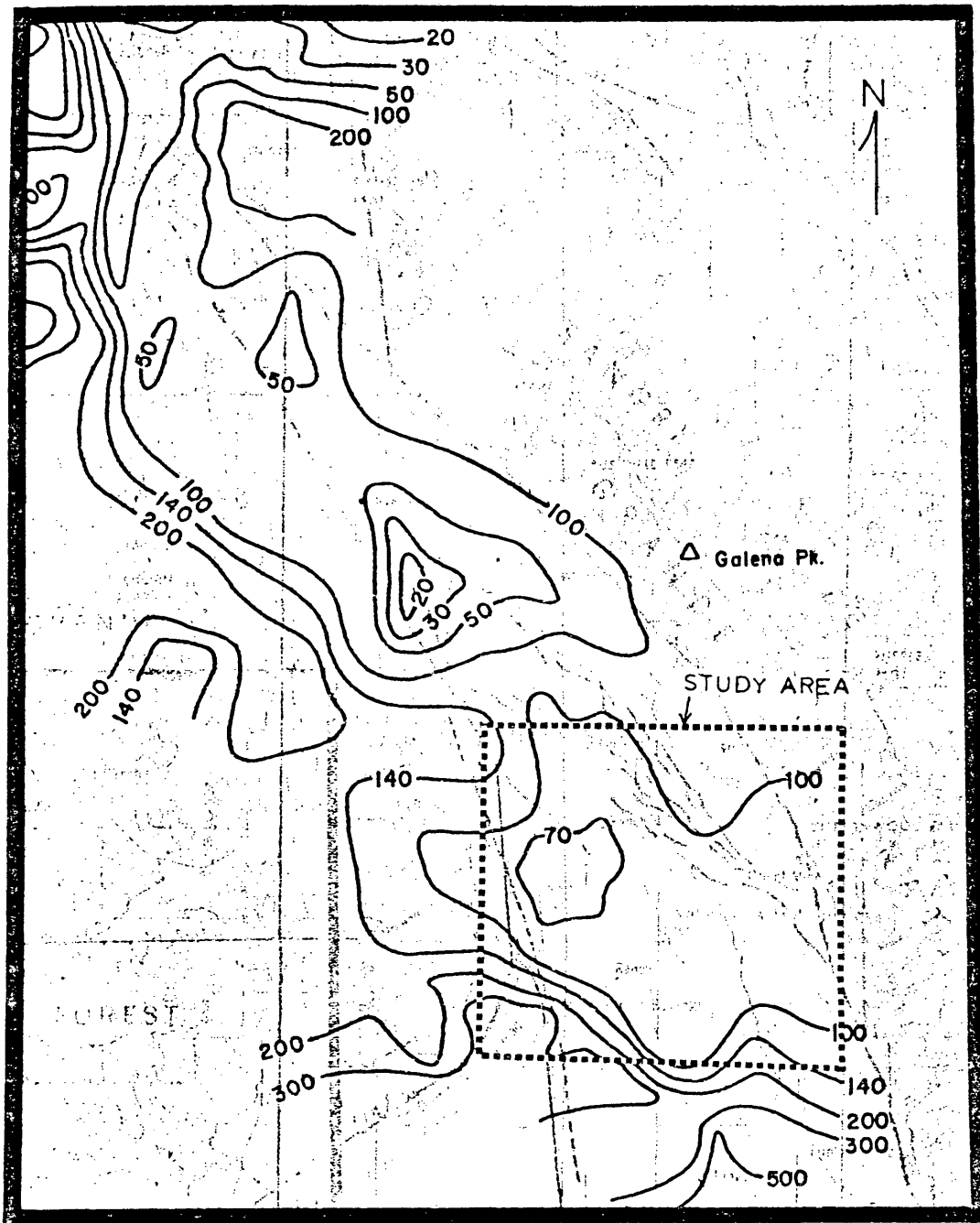


Figure 31. Apparent resistivity map (from Keller, in Romero and Fawcett, 1978). The contours are in ohm-meters.

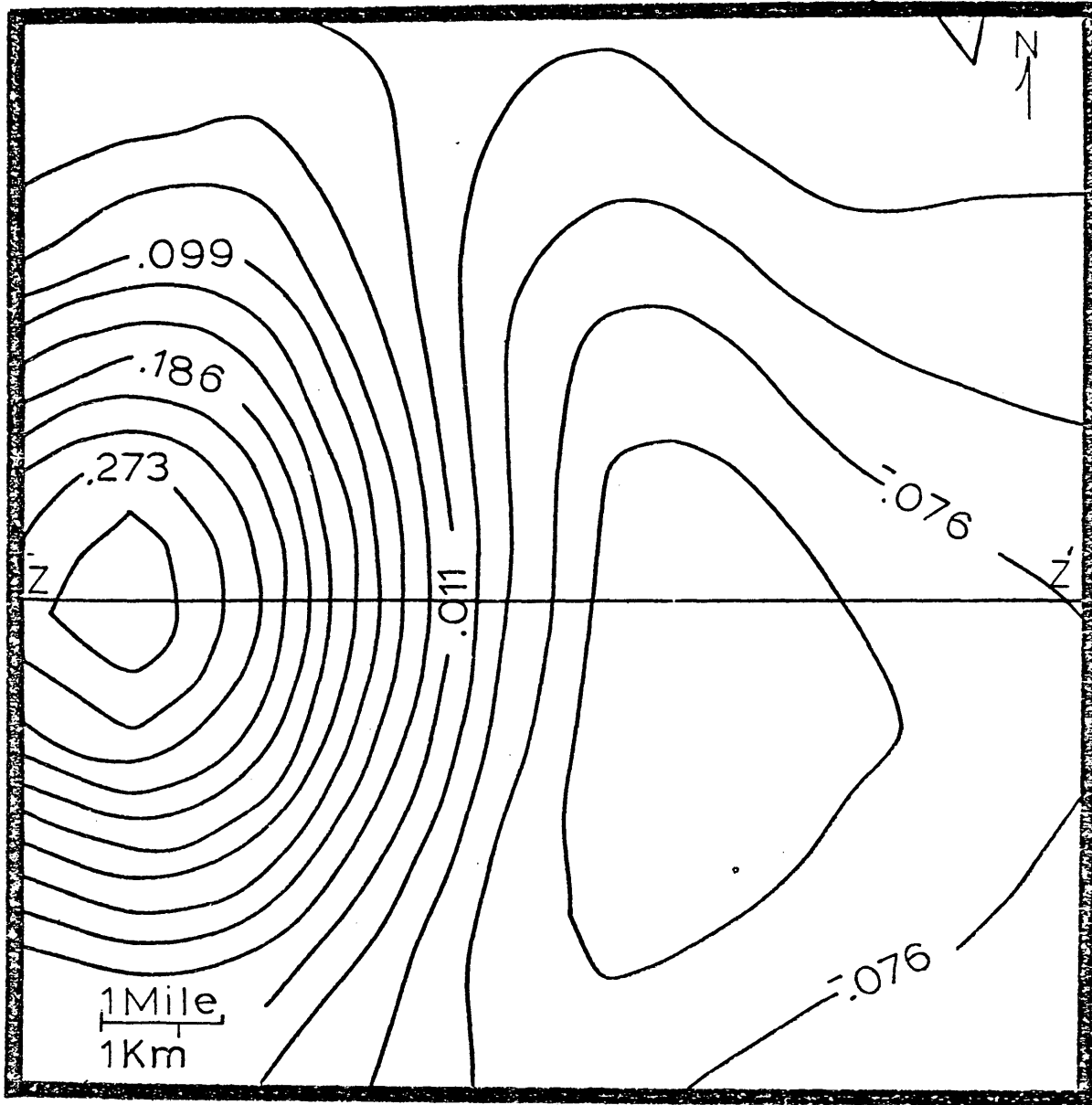


Figure 32. Sixth order surface continued down one mile.
The contour interval is 0.0291 volts. The
map is of the same area as the base map
(Figure 3).

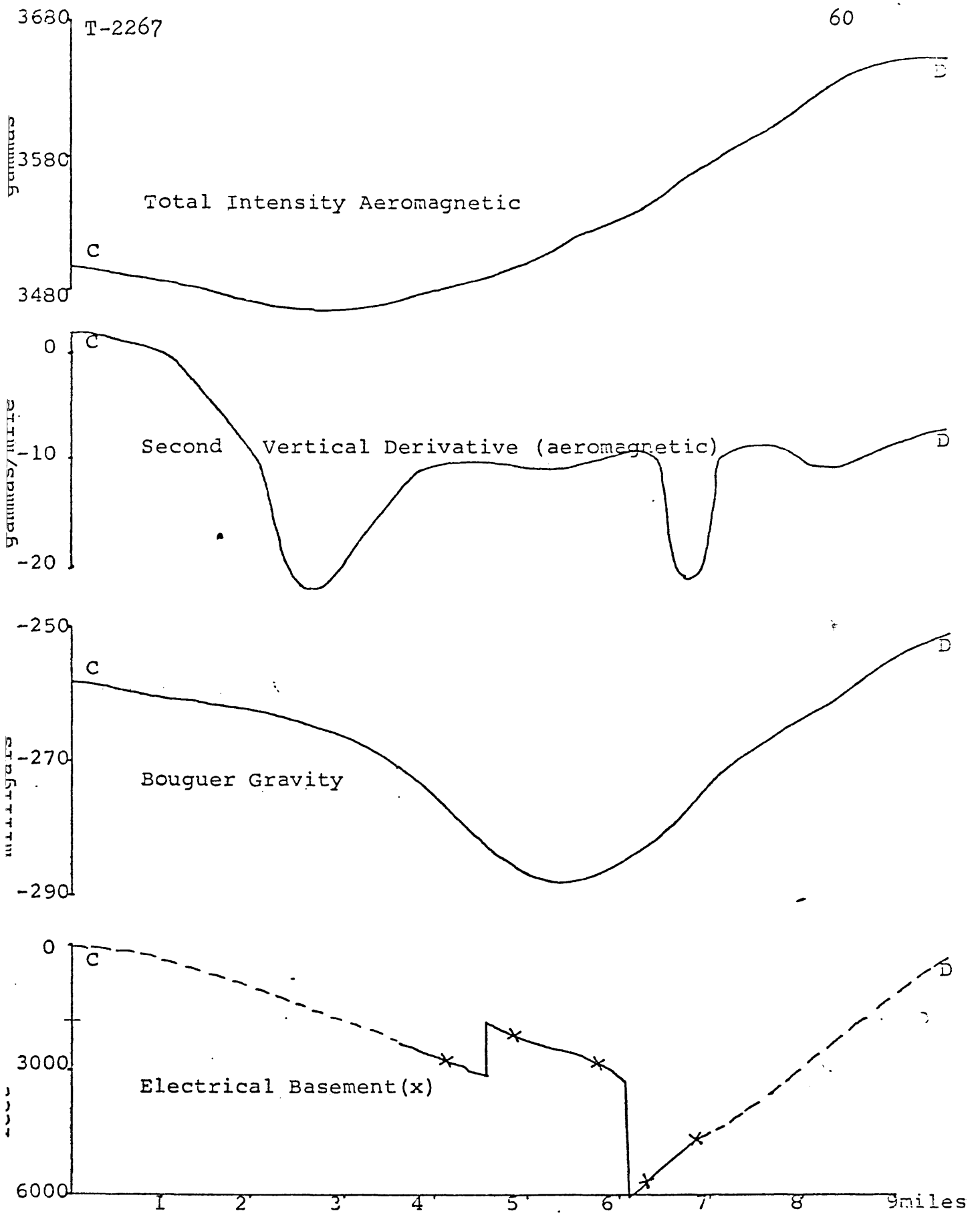


Figure 33. Correlation between aeromagnetic, second vertical derivative-aeromagnetic, Bouguer gravity, and electrical basement profiles (from Jordan, 1974).

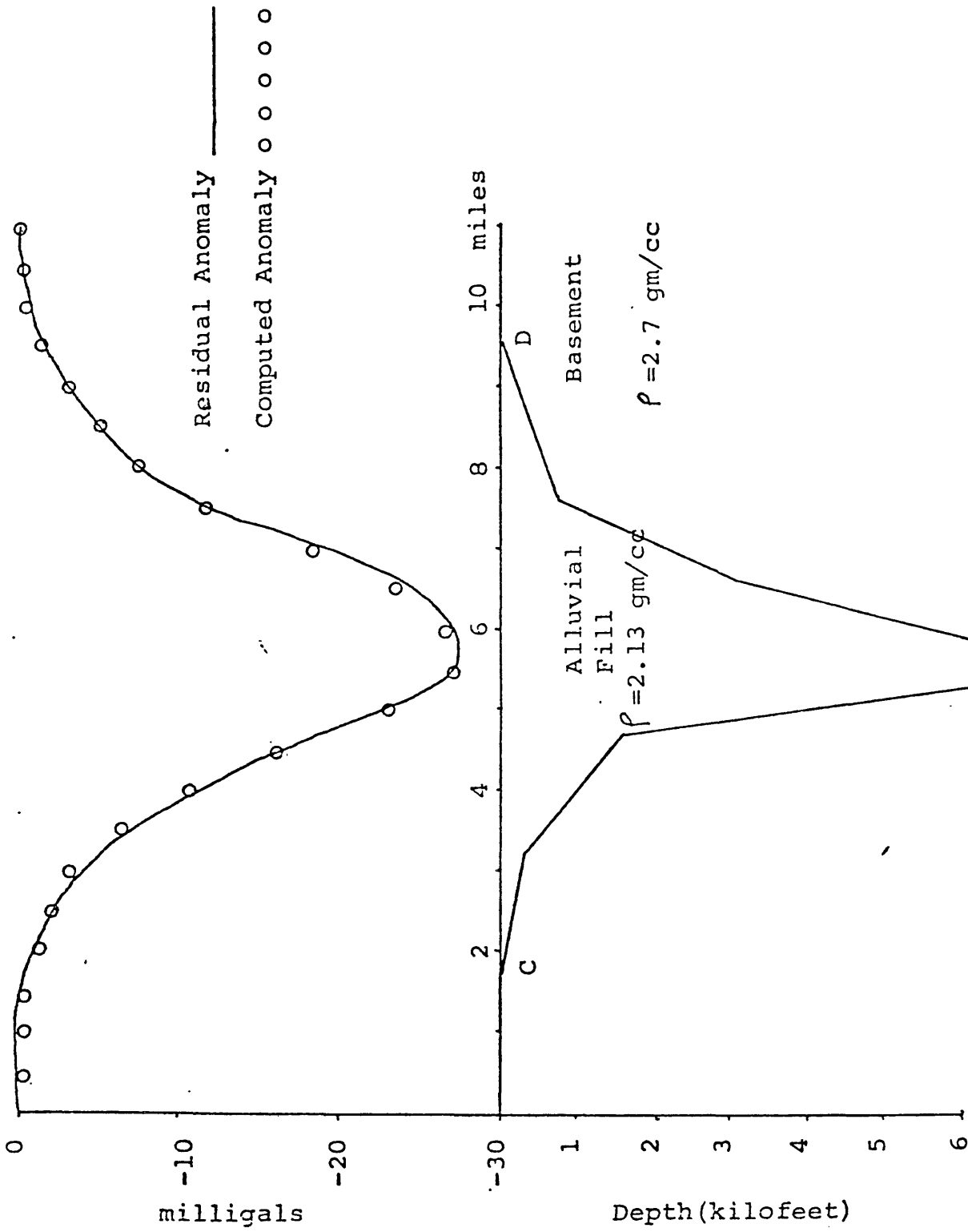


Figure 34. Residual gravity anomaly and geologic model (from Jordan, 1974).

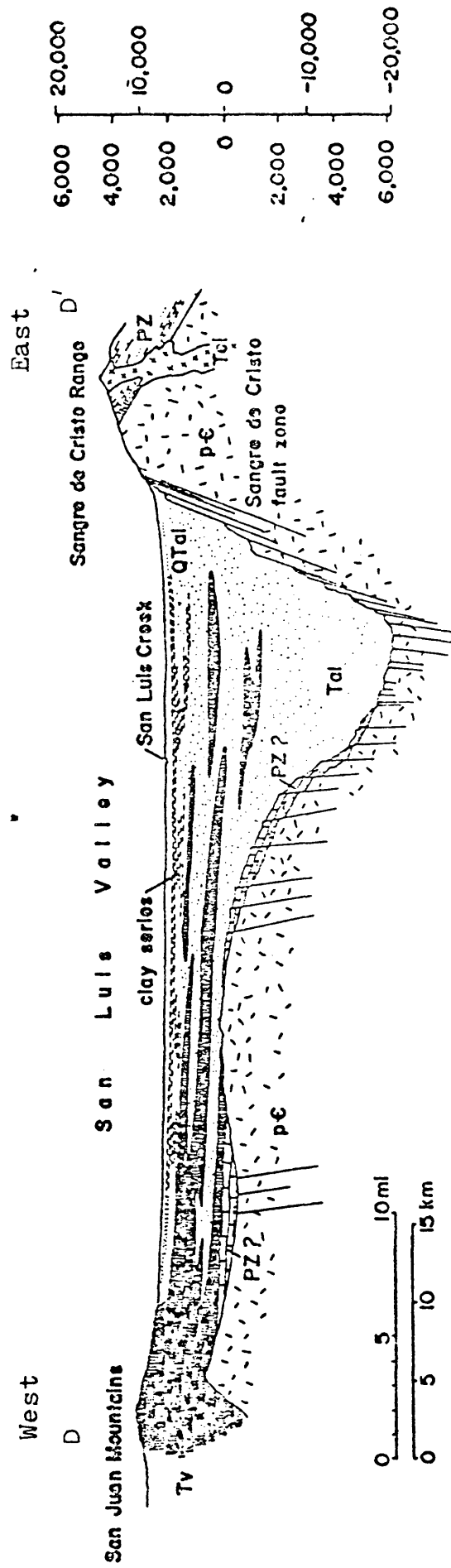
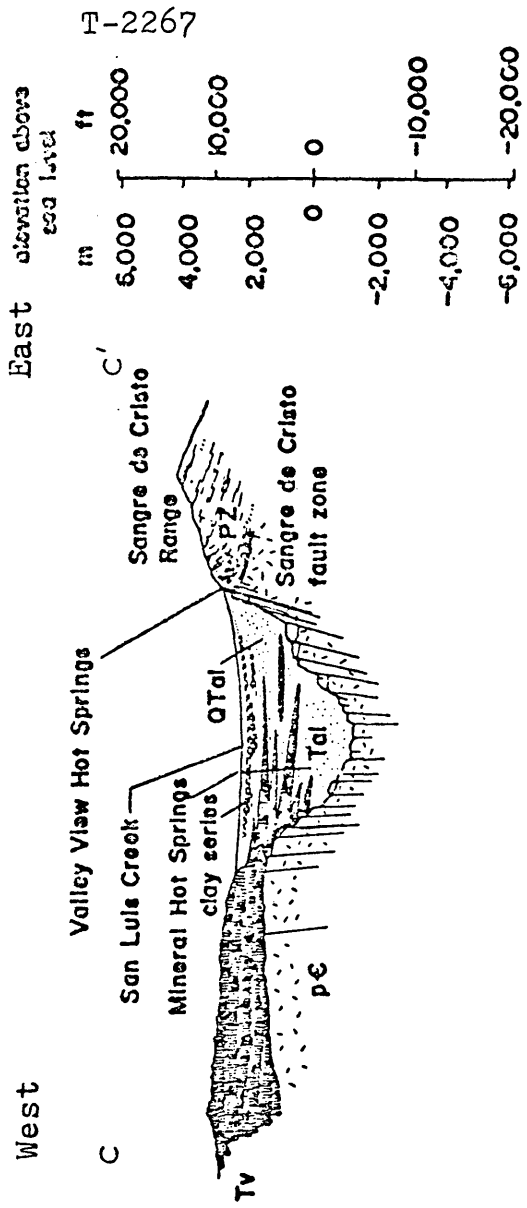


Figure 35. Geologic sections of the northern San Luis Valley (from Romero and Fawcett, 1978).

the filtered potential map (Figure 36) shows that the valley is shallow in the west, falling off at a steep angle to the deep part of the valley in the east. This assumes that there is a correlation between the values of the contours and depth. There is no representation in the map of the affect of the Sangre de Cristo fault, the subsurface contact of the valley floor and the Sangre de Cristo mountains. This lack of resolving the eastern edge of the valley is probably due to a lack of sufficient data in the eastern part of the area.

There are two fault systems, the Kerber Creek-Major Creek and the Villa Grove, that trend northwestward. The filtered maps were unable to delineate these zones. Also, a northwest trending horst in the basement (Stoughton, 1977; Jordan, 1974; and Romero and Fawcett, 1978) was not seen in the maps.

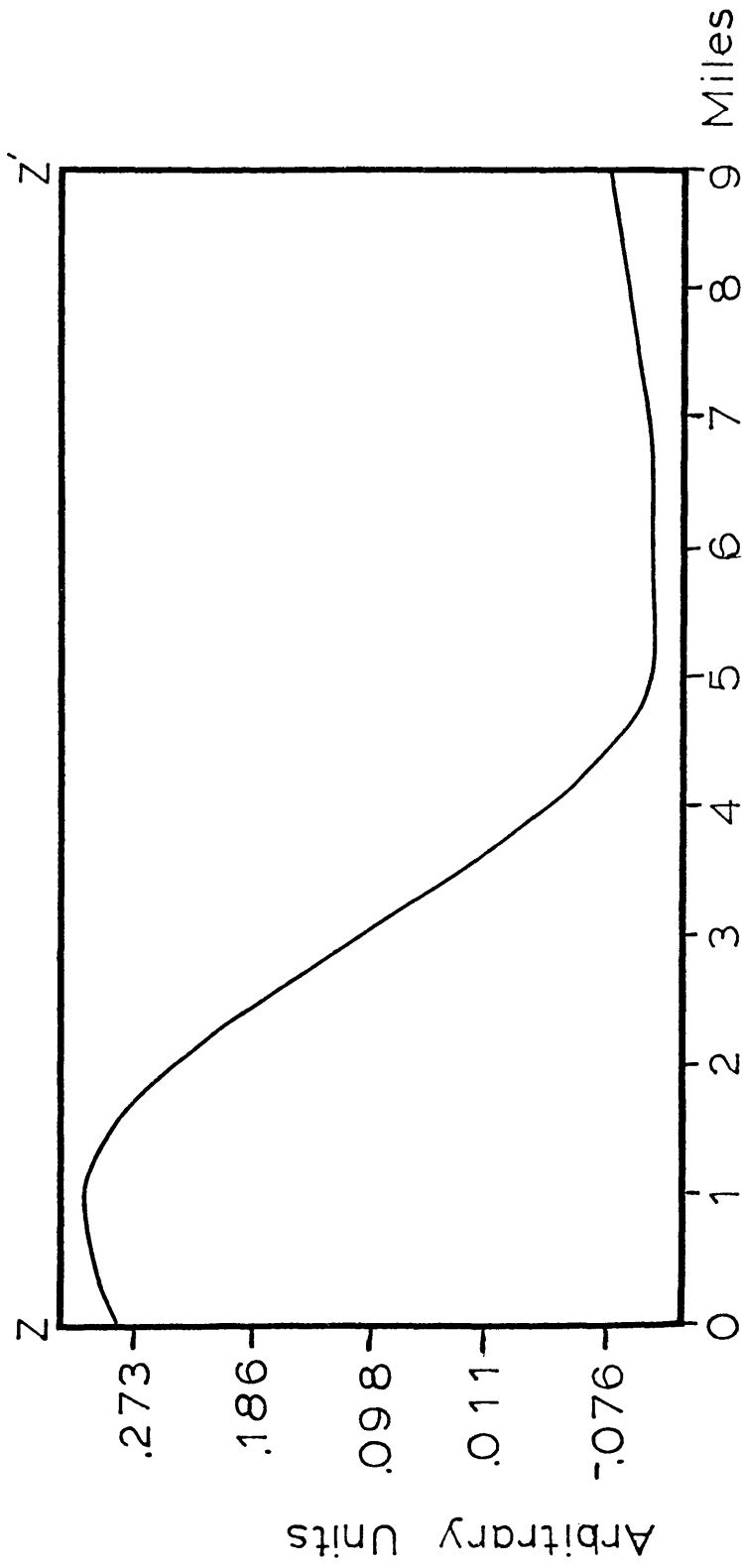


Figure 36. Crosssection of the sixth order surface continued down one mile.

CONCLUSIONS

Mapping of electrical potentials proved to be an effective method for determining the resistivity and subsurface structure. The field method is relatively quick and simple. Errors in the data did not prove to be too serious, and could be decreased by more care in the field procedure. The resistivity map generated from the potential gives as good or better results than the quadripole or bipole-dipole methods, though the geometric factor may cause erroneous values near the equator of the source.

Surface fitting of the potential resulted in being equivalent to a downward continuation. The sixth order surface was, in this case, probably the most representative of the subsurface. Filtering of the surfaces by using downward continuation filters resulted in removing some of the noise, but may also result in filtering out the anomaly. This poor control of what wavelengths are enhanced is a major drawback of how the filtering was done. The surface fitting and continuation were not able to resolve the finer structures of the basement.

If this method is to be pursued further, it will be necessary to improve on the field techniques, gridding techniques, and spatial filtering techniques. The field data would be improved by having a higher density of stat-

ions, and an even distribution of stations over the area. Gridding techniques using polynomials or Fourier methods would decrease the smoothing that occurs during gridding. Also, a finer grid spacing would enhance the shorter wavelengths, and allow the smaller structures to be seen.

Fourier analysis would give information about what wavelengths are enhanced and which are masked by both the surface fitting and continuation. The downward continuation could be improved by using shorter, more sophisticated filters. Other methods of spatial filtering should be used, these could be band-pass filtering, strike filtering (Fuller, 1967; Zurflueh, 1967), elliptical filters (Keller, 1979), or derivative operators (Peters, 1949; Fuller, 1967; and Bhattacharyya, 1976).

This study has shown that it is possible to map the potential due to a bipole source, and then to be able to use the methods of data processing and interpretation available from the gravitational and magnetic methods. The information added by the potential field data to the resistivity data can be an important improvement in the direct-current methods. But, with the improvements needed in data processing and modeling, it will still remain to be seen if the method is economically superior to the already existing direct-current methods.

APPENDIX 1

This appendix gives the station number, x-y coordinate, potential and current for each station. The station numbers (Sta.) are as they appear on plate 1, and are listed in the order of the summation of the potential differences. Due to the digitization of the map, the x-y units have the value of 7.8 meters, with the origin being the western source electrode (Plate 1). The potential values are those after summation of the potential differences and before normalizing by a factor of 10,000 and adding the constant of .0118. The current is in amperes.

APPENDIX I

Sta.	X	Y	Potential	Current
32	-376.0000	1030.0000	1.530000	108.0000
33	-356.0000	975.0000	3.190000	108.0000
32	-334.0000	965.0000	6.720000	109.0000
32	-312.0000	920.0000	11.260000	107.0000
31	-290.0000	397.0000	14.500000	111.0000
31	-269.0000	353.0000	19.020000	111.0000
30	-250.0000	325.0000	23.320000	111.4000
30	-234.0000	735.0000	31.320000	111.4000
29	-227.0000	754.0000	41.820000	107.0000
29	-224.0000	712.0000	56.520000	107.0000
28	-220.0000	673.0000	80.320000	103.0000
28	-217.0000	622.0000	108.320000	103.0000
927	-214.0000	573.0000	160.220000	107.0000
927	-211.0000	553.0000	226.470000	107.0000
27	-207.0000	513.0000	311.470000	107.0000
27	-207.0000	513.0000	311.470000	107.0000
26	-203.0000	473.0000	432.670000	107.0000
26	-199.0000	431.0000	566.370000	107.0000
25	-196.0000	391.0000	732.670000	107.0000
25	-192.0000	349.0000	893.070000	107.0000
24	-189.0000	310.0000	1112.070000	107.0000
24	-185.0000	267.0000	1352.070000	107.0000
23	-182.0000	213.0000	1714.070000	107.0000
22	-173.0000	192.0000	2067.070000	107.0000
922	-175.0000	150.0000	2580.550000	109.0000
922	-172.0000	109.0000	2964.550000	109.0000
22	-168.0000	70.000000	3017.930000	109.0000
22	-164.0000	30.000000	3306.930000	109.0000
1	-161.0000	-9.000000	3270.570000	109.0000
1	-160.0000	-54.000000	2868.570000	109.0000
2	-160.0000	-93.000000	2211.370000	108.0000
2	-166.0000	-130.0000	1825.970000	108.0000
3	-175.0000	-181.0000	1536.970000	109.0000
3	-183.0000	-220.0000	1456.070000	109.0000
4	-203.0000	-253.0000	1168.270000	109.0000
4	-221.0000	-292.0000	927.870000	109.0000
5	-240.0000	-328.0000	734.670000	109.0000
5	-259.0000	-364.0000	581.070000	109.0000
5	-277.0000	-400.0000	428.870000	103.0000
5	-295.0000	-435.0000	293.570000	108.0000
7	-317.0000	-471.0000	179.770000	108.0000
7	-339.0000	-502.0000	119.170000	108.0000
9	-368.0000	-532.0000	58.070000	112.0000
9	-396.0000	-559.0000	15.829930	112.0000
10	-431.0000	-536.0000	-75.529930	111.0000
10	-465.0000	-510.0000	-120.529930	111.0000

Sta.	X	Y	Potential	Current
11	-497.0000	-635.0000	184.0200	111.0000
11	-529.0000	-655.0000	190.5200	111.0000
12	-553.0000	-681.0000	194.6600	113.0000
12	-595.0000	-703.0000	199.0000	113.0000
13	-628.0000	-726.0000	205.2700	114.0000
13	-653.0000	-749.0000	214.3500	114.0000
14	-693.0000	-774.0000	227.2800	112.0000
14	-726.0000	-795.0000	242.4300	112.0000
15	-758.0000	-819.0000	258.5900	111.0000
15	-791.0000	-841.0000	267.8300	111.0000
16	-824.0000	-865.0000	273.3300	105.0000
16	-850.0000	-884.0000	283.1300	105.0000
18	-883.0000	-907.0000	293.3500	103.0000
18	-912.0000	-927.0000	293.3500	103.0000
19	-945.0000	-951.0000	326.0700	102.0000
19	-976.0000	-974.0000	338.6900	102.0000
20	-1010.0000	-993.0000	352.8200	102.0000
20	-1107.0000	-1059.0000	354.4400	102.0000
21	-1074.0000	-1045.0000	354.4400	104.0000
21	-1041.0000	-1021.0000	330.5400	104.0000
115	-331.0000	892.0000	17.45000	105.4000
115	-355.0000	875.0000	20.87000	105.4000
116	-410.0000	837.0000	23.45000	105.0000
116	-444.0000	859.0000	26.82000	105.0000
117	-475.0000	850.0000	31.17000	105.7000
117	-506.0000	829.0000	36.02000	105.7000
118	-538.0000	815.0000	42.99000	105.2000
118	-569.0000	802.0000	45.21000	105.2000
119	-609.0000	782.0000	55.31000	105.4000
119	-641.0000	769.0000	68.61000	105.4000
120	-674.0000	755.0000	78.81000	107.0000
120	-712.0000	745.0000	93.96000	107.0000
121	-751.0000	735.0000	144.4600	105.0000
121	-777.0000	727.0000	237.3300	105.0000
122	-807.0000	720.0000	253.6300	105.7000
122	-827.0000	715.0000	278.8200	105.7000
123	-855.0000	708.0000	288.4200	107.4000
123	-909.0000	699.0000	291.7500	107.4000
124	-944.0000	683.0000	293.3300	109.0000
124	-1001.0000	555.0000	301.5700	109.0000
125	-1055.0000	545.0000	303.1900	109.1000
125	-1035.0000	599.0000	289.8900	109.1000
126	-1125.0000	552.0000	275.7500	103.7000
126	-1201.0000	535.0000	224.2400	108.7000
127	-1273.0000	504.0000	134.1400	110.6000
127	-1315.0000	459.0000	148.5400	110.6000
128	-1357.0000	432.0000	129.8400	111.4000

Sta.	X	Y	Potential	Current
128	-1405.000	339.0000	100.3400	111.4000
129	-1481.000	348.0000	53.93000	110.5000
129	-1538.000	337.0000	32.73000	110.5000
130	-1539.000	341.0000	16.28000	109.0000
130	-1547.000	352.0000	1.730002	109.0000
131	-1713.000	375.0000	-7.309998	109.0000
131	-1765.000	410.0000	-17.91000	109.0000
132	-1813.000	448.0000	-22.03000	109.0000
132	-1852.000	491.0000	-26.82000	109.0000
133	-1870.000	538.0000	-33.99000	109.5000
133	-1941.000	590.0000	-42.27000	109.5000
134	-1980.000	640.0000	-48.33000	110.0000
134	-2017.000	636.0000	-55.90000	110.0000
135	-2068.000	731.0000	-63.78000	110.0000
135	-2110.000	771.0000	-71.22000	110.0000
301	-210.0000	831.0000	12.72000	110.5000
301	-182.0000	851.0000	5.720000	110.5000
302	-130.0000	855.0000	2.350000	112.5000
302	-87.00000	857.0000	-2.410000	112.5000
303	45.00000	860.0000	-7.410000	111.5000
303	0.0000000E+00	863.0000	-11.65000	111.5000
304	45.00000	873.0000	-15.82000	110.0000
304	45.00000	824.0000	-14.07000	110.0000
305	72.00000	825.0000	-20.87000	110.0000
305	120.0000	824.0000	29.07000	110.0000
306	152.0000	824.0000	-39.97000	110.0000
306	191.0000	824.0000	-50.97000	110.0000
307	232.0000	823.0000	-51.97000	110.0000
307	273.0000	823.0000	-72.27000	110.0000
308	313.0000	823.0000	-84.27000	109.5000
308	354.0000	823.0000	-97.07000	109.5000
309	394.0000	823.0000	-112.1700	109.0000
309	436.0000	823.0000	-126.9700	109.0000
310	474.0000	823.0000	-137.2700	114.5000
310	510.0000	820.0000	-151.3700	114.5000
311	514.0000	802.0000	-168.3700	114.0000
311	514.0000	757.0000	-183.2700	114.0000
312	513.0000	728.0000	-200.0700	115.0000
312	516.0000	696.0000	-223.2700	115.0000
313	512.0000	668.0000	-232.6100	115.0000
313	488.0000	636.0000	-233.4100	115.0000
314	488.0000	596.0000	-259.4100	114.5000
314	488.0000	554.0000	-285.7100	114.5000
315	488.0000	513.0000	-313.9100	110.5000
315	488.0000	472.0000	-345.7100	110.5000
316	488.0000	429.0000	-388.7100	110.0000
316	487.0000	389.0000	-437.4100	110.0000

Sta.	X	Y	Potential	Current
317	436.0000	350.0000	-492.2100	110.5000
317	436.0000	309.0000	-559.9100	110.5000
318	434.0000	270.0000	-639.7100	110.5000
318	434.0000	228.0000	-741.7100	110.5000
319	434.0000	181.0000	-875.0100	111.0000
319	434.0000	144.0000	-1030.510	111.0000
320	434.0000	111.0000	-1217.310	112.0000
320	433.0000	67.00000	-1418.310	112.0000
321	433.0000	31.00000	-1561.710	112.5000
321	433.0000	-3.000000	-1734.910	112.5000
322	523.0000	-8.000000	-1460.710	112.5000
322	564.0000	-8.000000	-1289.010	112.5000
9322	604.0000	-8.000000	-1175.910	110.0000
9322	644.0000	-8.000000	-1100.210	110.0000
323	634.0000	-8.000000	-1055.410	115.0000
323	726.0000	-8.000000	-1014.910	115.0000
324	766.0000	-9.000000	-932.8100	115.0000
324	806.0000	-9.000000	-951.5100	115.0000
325	846.0000	-9.000000	-943.0100	114.0000
325	837.0000	-9.000000	-928.3100	114.0000
326	928.0000	-11.00000	-915.8100	114.0000
326	963.0000	-9.000000	-901.6700	114.0000
327	1003.000	10.00000	-835.4700	115.0000
327	1045.000	-12.00000	-867.4700	115.0000
328	1063.000	-26.00000	-854.8700	115.0000
328	1039.000	-54.00000	-847.8700	115.0000
329	1120.000	-57.00000	-827.5700	115.0000
329	1144.000	-27.00000	-831.8100	115.0000
330	1167.000	-48.00000	-819.2100	115.5000
330	1193.000	-33.00000	-809.7100	115.5000
331	1241.000	-103.0000	-792.0100	116.0000
331	1257.000	-128.0000	-776.3100	115.0000
332	1273.000	-146.0000	-762.0100	103.0000
332	1284.000	-183.0000	-735.4100	103.0000
333	1293.000	-226.0000	-703.1100	103.0000
333	1287.000	-270.0000	-705.7100	103.0000
334	1284.000	-307.0000	-703.1100	107.0000
334	1291.000	-344.0000	-690.9100	107.0000
335	1293.000	-384.0000	-695.6100	107.5000
335	1293.000	-423.0000	-692.0100	107.5000
336	1294.000	-454.0000	-686.4100	107.5000
336	1294.000	-515.0000	-680.3100	107.5000
337	1294.000	-555.0000	-677.1300	107.0000
337	1278.000	-594.0000	-677.1800	107.0000
338	1244.000	-619.0000	-685.2600	103.0000
338	1181.000	-617.0000	-693.3400	103.0000

Sta.	X	Y	Potential	Current
339	1120.000	-616.0000	-708.1400	107.5000
339	1093.000	-616.0000	-710.0400	107.5000
340	1020.000	-640.0000	-716.0100	110.0000
340	1090.000	-673.0000	-708.0400	110.0000
341	1090.000	-709.0000	-701.8700	108.5000
341	1091.000	-749.0000	-695.8100	108.5000
63	1092.000	-791.0000	-690.1000	108.5000
63	1092.000	-824.0000	-682.2000	108.5000
52	1065.000	-825.0000	-688.2000	108.5000
62	1038.000	-824.0000	-698.5000	103.5000
61	1010.000	-825.0000	-700.3000	117.5000
61	977.0000	-825.0000	-702.2000	117.5000
60	942.0000	-825.0000	-702.2000	123.0000
60	907.0000	-825.0000	-702.2000	123.0000
59	872.0000	-824.0000	-702.6000	122.0000
59	834.0000	-825.0000	-704.4700	122.0000
58	802.0000	-825.0000	-703.8700	122.0000
58	767.0000	-825.0000	-702.5700	122.0000
57	732.0000	-826.0000	-701.0700	122.0000
57	698.0000	-826.0000	-698.3700	122.0000
56	662.0000	-826.0000	-699.0700	120.0000
56	627.0000	-826.0000	-702.6700	120.0000
55	593.0000	-827.0000	-704.3700	119.5000
55	553.0000	-829.0000	-710.9700	119.5000
54	517.0000	-829.0000	-715.9700	118.0000
54	482.0000	-829.0000	-722.5700	118.0000
53	482.0000	-796.0000	-720.1700	120.5000
53	482.0000	-764.0000	-700.2700	120.5000
52	482.0000	-734.0000	-703.6700	122.0000
52	482.0000	-703.0000	-692.4700	122.0000
51	482.0000	-675.0000	-685.3700	119.0000
51	482.0000	-643.0000	-673.2700	119.0000
50	482.0000	-612.0000	-664.9700	119.5000
50	482.0000	-571.0000	-662.5700	119.5000
49	456.0000	-571.0000	-672.1700	118.5000
49	424.0000	-571.0000	-687.9700	118.5000
48	392.0000	-571.0000	-697.7700	120.5000
48	362.0000	-571.0000	-718.8700	120.5000
47	332.0000	-571.0000	-707.7700	119.0000
47	296.0000	-571.0000	-699.5700	119.0000
46	261.0000	-571.0000	-663.3700	119.0000
46	229.0000	-572.0000	-629.9700	119.0000
44	198.0000	-572.0000	-531.9700	120.0000
44	168.0000	-573.0000	-534.7700	120.0000
43	128.0000	-571.0000	-480.5700	119.0000
43	91.00000	-569.0000	-432.0700	119.0000

Sta.	X	Y	Potential	Current
42	57.00000	-559.0000	384.3700	121.0000
42	18.00000	-570.0000	342.4700	121.0000
41	17.00000	-550.0000	305.9700	121.0000
41	17.00000	-550.0000	305.9700	121.0000
40	15.00000	-531.0000	214.3700	120.0000
40	11.00000	-489.0000	-159.5700	120.0000
39	7.000000	-452.0000	-52.57005	120.0000
39	2.000000	-412.0000	9.929955	120.0000
38	-1.000000	-372.0000	169.9300	119.5000
38	-6.000000	-329.0000	262.2300	119.5000
37	-8.000000	-293.0000	530.1300	118.5000
37	-13.00000	-263.0000	664.1300	118.5000
925	-19.00000	-234.0000	1353.930	118.0000
925	-30.00000	-205.0000	1674.330	118.0000
35	-49.00000	-176.0000	2520.230	116.5000
35	-72.00000	-142.0000	3063.330	116.5000
35	-95.00000	-109.0000	3315.030	116.5000
35	-116.0000	-80.00000	3761.430	116.5000
34	-142.0000	-45.00000	3612.530	118.5000
34	-161.0000	-10.00000	3514.130	118.5000
114	-216.0000	786.0000	34.25000	118.0000
114	-189.0000	763.0000	26.37000	118.0000
113	-168.0000	751.0000	40.37000	118.0000
113	-147.0000	736.0000	42.69000	118.0000
112	-125.0000	722.0000	57.44000	118.0000
112	-111.0000	500.0000	70.87000	118.0000
111	-99.00000	671.0000	91.87000	118.0000
111	-89.00000	533.0000	117.8700	118.0000
110	-84.00000	599.0000	173.3700	118.0000
110	-81.00000	560.0000	224.1700	118.0000
109	-78.00000	518.0000	307.9700	121.5000
109	-72.00000	466.0000	409.9700	121.5000
108	-67.00000	419.0000	560.4700	121.0000
108	-63.00000	378.0000	711.9700	121.0000
107	-59.00000	340.0000	927.0700	122.0000
107	-55.00000	300.0000	1154.270	122.0000
106	-51.00000	260.0000	1458.270	120.0000
106	-47.00000	220.0000	1781.220	120.0000
355	-42.00000	180.0000	2262.620	117.0000
355	-43.00000	180.0000	2262.620	117.0000
354	-40.00000	142.0000	2895.820	117.0000
354	-35.00000	100.0000	3985.320	117.0000
353	-35.00000	61.00000	7474.820	117.0000
353	-27.00000	20.00000	12115.42	117.0000
352	-40.00000	0.0000000E+00	15652.42	118.0000
352	-78.00000	0.0000000E+00	9330.420	118.0000

Sta.	X	Y	Potential	Current
351	-120.0000	0.000000E+00	.6574.820	117.5000
351	-161.0000	-9.000000	5044.620	117.5000
348	482.0000	-31.00000	-1227.410	118.5000
348	482.0000	-42.00000	-1187.010	118.5000
347	481.0000	-72.00000	-1007.210	119.5000
347	481.0000	-112.0000	849.6100	119.5000
346	481.0000	-153.0000	-736.5100	119.0000
346	481.0000	-196.0000	-645.9100	119.0000
345	481.0000	-235.0000	-573.3100	121.0000
345	481.0000	-277.0000	-526.2100	121.0000
344	482.0000	-326.0000	-489.7100	121.0000
344	482.0000	-375.0000	-457.6100	121.0000
343	483.0000	-426.0000	-435.8100	121.0000
343	482.0000	-474.0000	-414.7100	121.0000
342	482.0000	-527.0000	-393.7100	120.5000
342	481.0000	559.0000	-384.4100	120.5000
357	35.000000	519.0000	275.3700	121.0000
357	5.000000	518.0000	244.4700	121.0000
353	44.00000	517.0000	218.5700	114.0000
353	33.00000	516.0000	187.2700	114.0000
359	127.0000	515.0000	147.8700	114.0000
359	167.0000	514.0000	117.5700	114.0000
360	194.0000	514.0000	78.17000	114.0000
360	221.0000	486.0000	67.87000	114.0000
361	225.0000	449.0000	65.27000	114.0000
361	225.0000	399.0000	55.17000	114.0000
362	225.0000	361.0000	69.97001	113.5000
362	223.0000	319.0000	34.97001	113.5000
363	250.0000	296.0000	43.57000	118.0000
363	263.0000	256.0000	21.47001	118.0000
364	277.0000	213.0000	-137.7300	116.0000
364	278.0000	177.0000	-202.2300	116.0000
365	274.0000	132.0000	-539.6300	115.0000
365	276.0000	86.00000	-1077.930	115.0000
366	272.0000	36.00000	-1938.430	118.5000
366	272.0000	0.000000E+00	1938.430	118.5000
349	442.0000	-6.000000	-2555.010	116.5000
349	404.0000	-5.000000	-6115.010	116.5000

REFERENCES

- Alfano, L., 1959, Introduction to the interpretation of resistivity measurements for complicated structural conditions: Geophysical Prospecting, v. 7, p. 311-366.
- Alpin, L. M. and others, 1966, Dipole methods for measuring earth conductivity: New York, Consultants Bureau, 177 p.
- Arestad, John F., 1977, Resistivity studies in the upper Arkansas Valley and Northern San Luis Valley, Colorado: Thesis T-1934, Colorado School of Mines, Golden, Colorado.
- Barnett, Colin T., 1972, Theoretical modelling of induced polarization effects due to arbitrarily shaped bodies: Thesis T-1453, Colorado School of Mines, Golden, Colorado.
- Bhattacharyya, B. K., 1969, Bicubic spline interpolation as a method for treatment of potential field data: Geophysics, v. 34, n. 3, p. 402-423.
- _____, 1976, Recursion filters for digital processing of potential field data: Geophysics, v.41, n. 4, p. 712-726.
- Crain, I. K. and Bhattacharyya, B. K., 1967, Treatment of non-equispaced two-dimensional data with a digital computer: Geoexploration, v. 5, p. 173-194.
- Dean, William C., 1958, Frequency analysis for gravity and magnetic interpretation: Geophysics, v. 23, n. 1, p. 97-127.
- Fuller, B. D., 1967, Two-dimensional frequency analysis and design of grid operators, in Mining geophysics, v. 2 : Tulsa, Society of Exploration Geophysicists, p. 658-708.
- House, Nancy Jo, 1979, Modified bipole-dipole survey, Belle Creek oil field: Thesis T-2203, Colorado School of Mines, Golden, Colorado.
- Jordan, John M., 1974, Geothermal investigations in the San Luis Valley, South-central Colorado: Thesis T-1478, Colorado School of Mines, Golden, Colorado.

- Keller, G. V., 1966, Dipole method for deep resistivity studies: *Geophysics*, v. 31, n. 6, p. 1088-1104.
- _____, 1978, Personal communication.
- _____, 1979, Personal communication.
- Keller, George V. and Frischknecht, Frank C., 1966, *Electrical methods in geophysical prospecting*: Oxford, Pergamon Press, 517 p.
- Keller, George V. and others, 1975, The dipole mapping method: *Geophysics*, v. 40, n. 3, p. 451-472.
- Kellogg, Oliver Dimon, 1929, *Foundations of potential theory*: New York, Dover, 384 p.
- Knepper, Daniel H., 1974, Tectonic analysis of the Rio Grande rift zone, central Colorado: Thesis T-1593, Colorado School of Mines, Golden, Colorado.
- Mamah, Luke I., 1979, The influence of finiteness of source on time domain electromagnetic soundings: Thesis T-2222, Colorado School of Mines, Golden, Colorado.
- Peters, Leo J., 1949, Direct approach to magnetic interpretation and its practical application: *Geophysics*, v. 14, n. 3, p. 290-320.
- Romero, John and Fawcett, Donald, 1978, Geothermal resources of south central Colorado and their relationship to ground and surface waters: State of Colorado Department of Natural Resources, Denver, Colorado, 127 p.
- Roy, Amalendu, 1966, Downward continuation and its application to electromagnetic data interpretation: *Geophysics*, v. 31, n. 1, p. 167-184.
- Simpson, Stephen M., 1954, Least squares polynomial fitting to gravitational data and density plotting by digital computers: *Geophysics*, v. 19, n. 2, p. 255-269.
- Stoughton, Dean, 1977, Interpretation of seismic reflection data from the San Luis Valley, south-central Colorado: Thesis T-1960, Colorado School of Mines, Golden, Colorado.
- Zohdy, Adel A. R., 1978, Total field resistivity mapping and sounding over horizontally layered media: *Geophysics*, v. 43, n. 4, p. 748-766.

Zurflueh, Ernst,G., 1967, Applications of two-dimensional linear wavelength filtering: geophysics, v. 32, n. 6, p. 1015-1035.

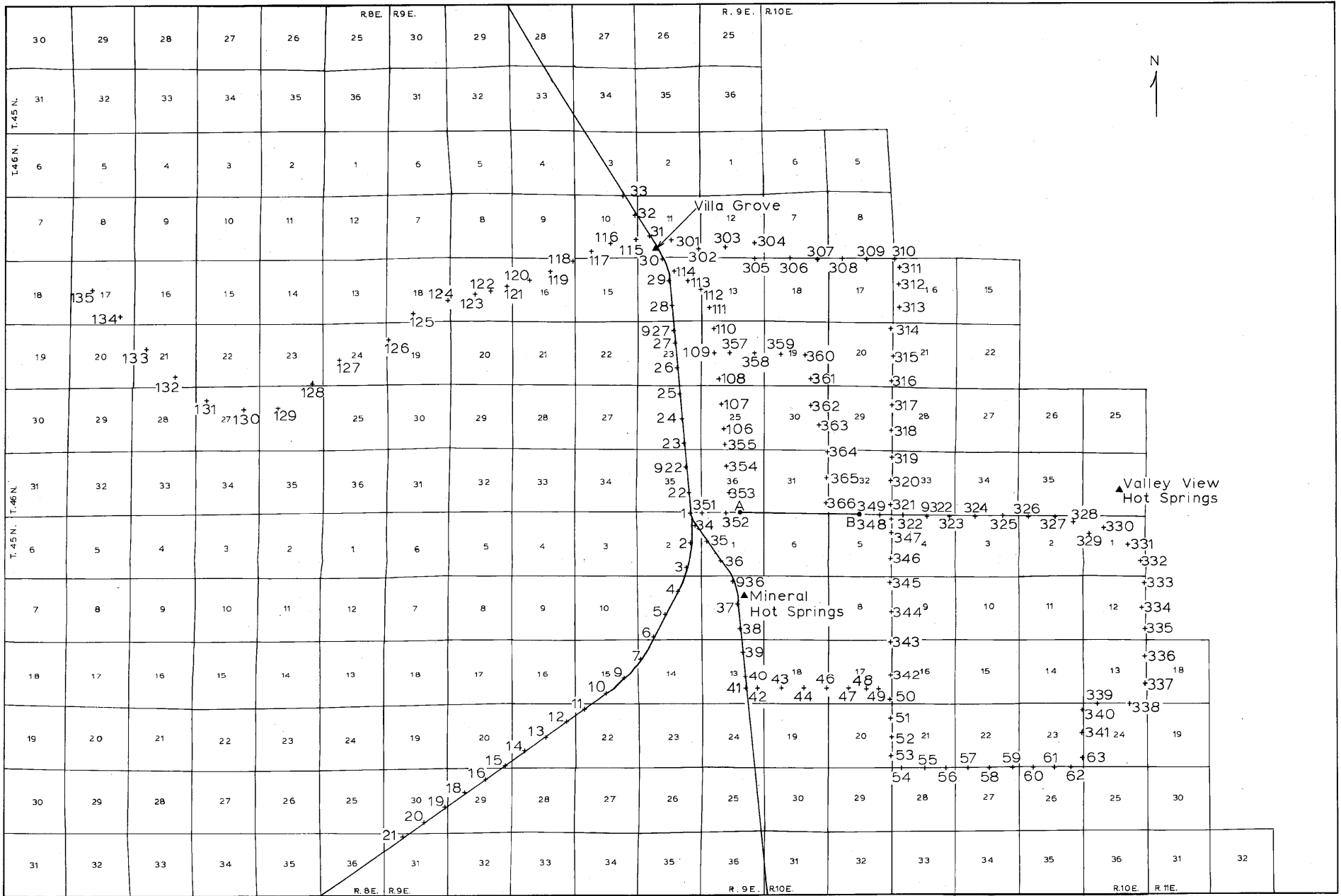


Plate 1. Station location map for electrical potential investigation of the San Luis Valley, Colorado.

Station location +
 Station number 123
 Source AB

0 1 2 3 Miles
 0 1 2 3 Km